Journal of Volcanology and Geothermal Research 119 (2002) 21–50
Journal of volcanology and geothermal research
www.elsevier.com/locate/jvolgeores

# Flux versus decompression melting at stratovolcanoes in southeastern Guatemala

B.I. Cameron [a,*], J.A. Walker [a], M.J. Carr [b], L.C. Patino [c], O. Matías [d], M.D. Feigenson [e]

[a] Department of Geology and Environmental Geosciences, Northern Illinois University, DeKalb, IL 60115-2854, USA
[b] Department of Geological Sciences, Rutgers University, Piscataway, NJ 08854-8066, USA
[c] Department of Geological Sciences, Michigan State University, East Lansing, MI 48824-1115, USA
[d] Instituto Nacional de Sismologia, Vulcanologia, Meteorologia e Hydrologia (INSIVUMEH), 7A Avenida 14-57, Zona 13, Guatemala City, Guatemala
[e] Department of Geological Sciences, Rutgers University, Piscataway, NJ 08854-8066, USA

Received 8 March 2002; accepted 13 March 2002

## Abstract

The major and trace element geochemistry of lavas erupted from four volcanic front (VF) stratovolcanoes in southeastern Guatemala show differences in the relative importance of flux and decompression melting in a continental arc setting. The VF stratovolcanoes exhibit a wide compositional range from basalt to dacite, although modern Pacaya erupts basaltic lavas. The VF basalts have relatively low MgO contents and plot outside the field of primary arc magmas defined by melting experiments on hydrous peridotite. After subtracting the effects of the fractionation, assimilation, and alteration of some VF lavas, separate partial melting and mixing trends were identified for Agua–Pacaya and Tecuamburro–Moyuta.

The distinct chemical signatures of the hemipelagic and carbonate sediments subducted off Guatemala provide constraints on material transfer processes that occurred between the slab and mantle wedge. Model fluids and melts from the subducted slab were calculated using recently published mineral–aqueous fluid partition coefficients. Wide separation of the model fluid and melt compositions on a U/La versus Ba/Th diagram creates diagnostic mixing curves with an enriched mid-ocean ridge basalt source. Fluid from mature ocean crust has high U/La, fluid from carbonate sediment has high Ba/Th, and fluid and melt from hemipelagic sediments have both high U/La and Ba/Th. In a simple single-stage model, a mantle metasomatized by fluid originating largely from the oceanic crust with only minor sediment fluid contributions best explains the overall large ion lithophile element composition of the VF lavas. $(Th/Rb)_N$ ratios of $\sim 1$ in the VF lavas from southeastern Guatemala require a component of sediment melting. Therefore, a more realistic two-stage model to describe the Guatemalan arc data involves an initial hemipelagic sediment melt input to the wedge followed by minor fluid additions from the oceanic crust or sediments. Correlation between measures of slab input and extent of melting in the older VF lavas from Tecuamburro and Moyuta favors flux-dominated melting near the base of the mantle wedge. In sharp contrast, the lack of a relationship between slab additions and melting in younger lavas from Agua and Pacaya volcanoes implies a significant role for decompression

* Corresponding author. Present address: Department of Geosciences, University of Wisconsin-Milwaukee, P.O. Box 413, Milwaukee, WI 53201, USA. Tel.: +1-414-229-3136; Fax: +1-414-229-5452.
*E-mail address:* bcameron@uwm.edu (B.I. Cameron).


PII: S0377-0273(02)00304-9

melting closer to the top of the wedge. In this melting scenario, the rate of crustal extension determines the extent of melting.


*Keywords:* Guatemala; stratovolcanoes; subduction zones; partial melting; magmas; geochemistry

## 1. Introduction

Arc lavas typically have enrichments in large ion lithophile elements (LILE) and depletions in high field strength elements (HFSE) relative to elements of similar incompatibility (Fig. 1a). The characteristic arc geochemical fingerprint reflects distinct melting processes or sources associated with subduction. Whereas mid-ocean ridge (MORB) and ocean island basalts (OIB) form by decompression melting (e.g. Langmuir et al., 1992; McKenzie and O'Nions, 1998), flux melting likely generates most arc magmas (e.g. Iwamori, 1998). High $H_2O$ contents measured in melt inclusions hosted by olivines from arc lavas (Sisson and Layne, 1993; Sobolev and Chaussidon, 1996; Roggensack et al., 1997) are evidence that fluids and/or melts evolve from the subducted slab (i.e. both sediments and oceanic crust), depress the solidus of the mantle wedge, and induce melting. However, very low $H_2O$ contents in volcanic front (VF) lavas from the Cascades in the western USA and Galunggung in Indonesia demonstrate a role

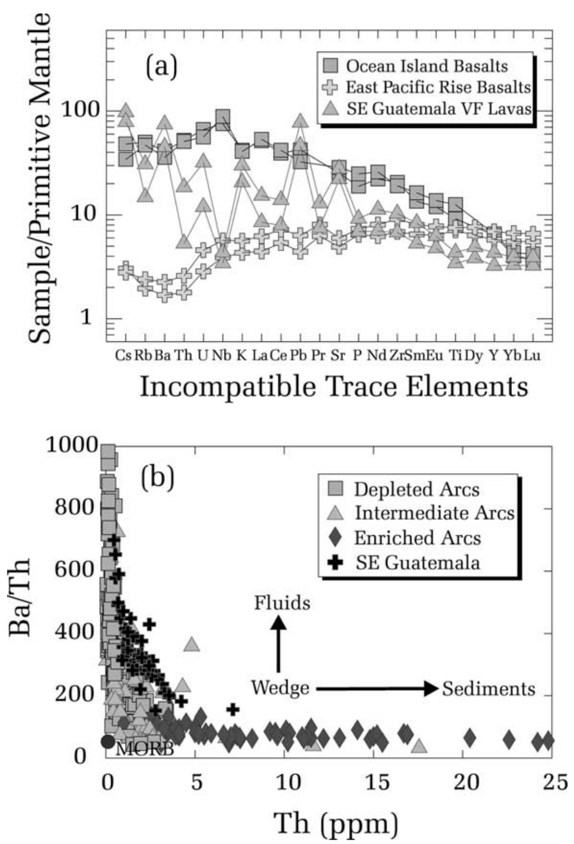


Fig. 1. (a) Primitive mantle-normalized trace element diagram depicts the sharp contrast in the chemical composition of basalts from three different tectonic settings. Samples were normalized to the primitive mantle of Sun and McDonough (1989). Basalt samples PH52-2 and PH72-3 from the East Pacific Rise (Regelous et al., 1999) show depletions in most of the highly incompatible trace elements relative to arc lavas from southeastern Guatemala. OIB samples from two of the Balleny Islands in the Southern Ocean (Berg et al., 1995) display enrichments in most of the highly incompatible elements relative to subduction zone magmas. The basaltic samples from Agua and Tecuamburro volcanoes in Guatemala exhibit the characteristic arc geochemical signature of enrichments in LILE such as Cs, Ba, U, and Pb, along with depletions in HFSE such as Nb and Ti. This distinct chemistry likely results from a melting process specific to the subduction setting. (b) The Ba/Th versus Th diagram helps define the different flavors of arc magmas (Hawkesworth et al., 1997). Trace element-depleted arcs such as the Marianas (Elliot et al., 1997), New Britain (Woodhead et al., 1998), Tonga-Kermadec (Turner et al., 1997), and Vanuatu (Peate et al., 1997) have high LILE/HFSE ratios owing to the mobilization of LILE from the downgoing slab. Arc magmas from the Aeolian Islands (Francalanci et al., 1993; Gertisser and Keller, 2000), Indonesia (Gerbe et al., 1992; Hoogewerf et al., 1997), and the Philippines (Bau and Knittle, 1993) have high Th concentrations from sediment contributions to the mantle wedge, and make up the trace element-enriched group. Intermediate arc magmas such as those from Kamchatka (Turner et al., 1998) and the Lesser Antilles (Turner et al., 1996) plot near MORB with low Ba/Th ratios and Th contents. The VF lavas from southeastern Guatemala exhibit a vertical trend suggesting derivation from a trace element-depleted mantle source.

for decompression melting beneath some subduction stratovolcanoes (Sisson and Layne, 1993; Sisson and Bronto, 1998). Large $^{231}$Pa excesses measured in recent U-series disequilibria studies of arc lavas also provide independent support for a component of decompression melting (Bourdon et al., 1999). These contrasting observations on the relative importance of flux and decompression melting serve as impetus for detailed examinations of the nature of mantle wedge melting at specific subduction zones.

Arc magmas exhibit significant compositional variability. Hawkesworth et al. (1997) classified arc lavas as either depleted or enriched based on their incompatible element chemistry (Fig. 1b). The depleted arc rocks have high LILE/HFSE ratios. LILE mobilized in hydrous fluids liberated from the subducted slab more effectively modify a depleted mantle source than an enriched one. On the other hand, enriched arc lavas with higher Th contents likely contain a greater contribution from subducted sediments (Hawkesworth et al., 1997). Notably, lavas from Central America were omitted from consideration owing to the U- and Ba-rich character of the subducted sediments. Instead of a hindrance, the distinct chemistry of the subduction inputs in Central America offers an unprecedented opportunity to track material transfer from the slab to the overlying mantle wedge in subduction zones and evaluate the melting process. Moreover, the protracted activity of front stratovolcanoes in southeastern Guatemala (Reynolds, 1987) allows the evaluation of lithological and chemical changes in the slab inputs since the Miocene.

The depletion of HFSE in arc rocks compared to MORB remains controversial (Ryerson and Watson, 1987; Keleman et al., 1993; Ewart and Hawkesworth, 1987). One attractive explanation involves episodes of melt extraction in the back-arc region followed by advection of depleted residual material into the arc source region and melting (Woodhead et al., 1993, 1998). One test of this model is to compare the chemistry of subduction zones with and without back-arc volcanism. Arc regions with a depleted character such as New Britain and Tonga have rapid convergence rates and well-developed back-arc regions (Woodhead et al., 1998). Furthermore, in the Kamchatkan arc, the most depleted VF rocks lie adjacent to zones that have chains of behind-the-front volcanoes (Hochstaedter et al., 1996a). Another test of this hypothesis is an examination of the temporal evolution of arc and back-arc systems (Davidson, 1996). Activity at front volcanoes in southeastern Guatemala has occurred both before and after pervasive Quaternary behind-the-front volcanism, and therefore potentially provides insight into the main cause of HFSE depletion in arc rocks.

## 2. Regional geological context

The VF of Central America, the trenchward limit of volcanism, extends for 1100 km from the Mexico–Guatemala border to central Costa Rica and includes at least 40 major volcanic centers (Carr and Stoiber, 1990). Stratovolcanoes of the VF form as a direct manifestation of subduction of the oceanic Cocos plate beneath the overriding Caribbean plate. The 26-km spacing of volcanic edifices represents one of the highest volcano densities amongst subduction zones (Carr and Stoiber, 1990). Subduction parameters such as crustal thickness, angle of subduction, and convergence rate presumably control the thermal structure of the subduction zone, and consequently influence the generation of arc magmas (Davies and Stevenson, 1992). Crustal thickness ranges from 48 km in northwestern Guatemala to 32 km in Nicaragua (Carr et al., 1990). Southeastern Guatemala has an intermediate crustal thickness of about 40 km (Carr et al., 1990). Whereas the Cocos plate subducts beneath Nicaragua at the steep angle of 65–84° (Carr et al., 1990; Protti et al., 1995), the angle of subduction lies closer to 40° in Guatemala. Convergence rate along the arc varies from 70 mm/yr in Guatemala to 90 mm/yr in Costa Rica (Demets et al., 1990).

Structural, geophysical, and geological features warrant division of the Central American arc into eight volcanic segments (Carr, 1984). Zones of transverse faulting separate these volcanic segments. Guatemala hosts three segments: the northwestern, central, and southeastern Guatema-

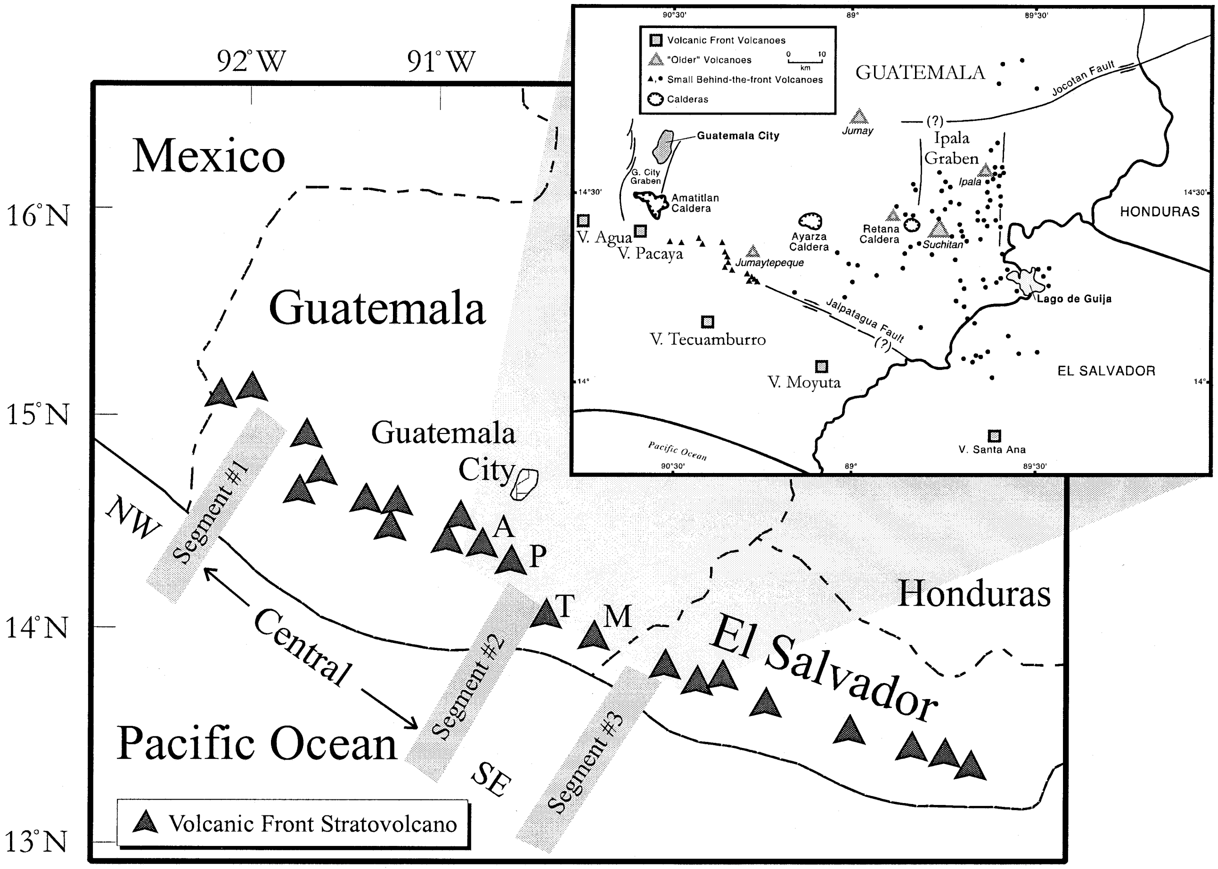


Fig. 2. Location map for the four VF stratovolcanoes examined in this geochemical study. Agua (A) and Pacaya (P) volcanoes occur in the central Guatemala segment of the Central America arc, whereas Tecuamburro (T) and Moyuta (M) occupy the southeastern Guatemala segment. Inset: a magnified view of the volcanological setting of southeastern Guatemala. Abundant behind-the-front volcanism lies adjacent to the four VF stratovolcanoes. Older BVF volcanism includes stratovolcanoes such as Ipala and Suchitan and calderas such as Retana and Ayarza. Younger BVF volcanism includes cinder cones that cluster in the Ipala Graben or along the trend of the Jalpatagua fault and shield volcanoes such as Las Viboras near Lago de Guija on the border with El Salvador. Note that Pacaya volcano occurs at the intersection of the Guatemala City graben and the projected Jalpatagua fault.

la volcanic segments (Fig. 2). Four volcanic centers (Agua, Pacaya, Tecuamburro, and Moyuta) constitute the VF in southern Guatemala; Agua and Pacaya from the central segment and Tecuamburro and Moyuta from the southeastern volcanic segment (Fig. 2). Southeastern Guatemala also hosts the most abundant behind the VF (BVF) volcanism in Central America. Over 200 cinder cones extend up to 120 km behind the front in southeastern Guatemala and northwestern El Salvador (Fig. 2).

The two central segment stratovolcanoes have been more recently active than their counterparts in the southeastern segment. Although Agua has not erupted historically, its near-perfect cone shape with the intact flanks lacking erosional incision suggests geologically recent volcanic activity. Current activity at the Mackenney cone of modern Pacaya alternates between Strombolian eruptions with effusion of small aa lava flows and more explosive Vulcanian blasts. Whereas ancestral Pacaya consists of both an andesitic composite volcano and a rhyodacitic dome, modern Pacaya has erupted lavas of progressively more

Table 1
Major element chemistry of lavas from VF stratovolcanoes (recalculated to 100%)

| Sample | GAG.01 | GAG.02 | GAG.03 | GAG.04 | GAG.06 | GAG.07 | GAG.08 | GAG.09 | GAG.10 | GAG.11 | GAG.12 |
|---|---|---|---|---|---|---|---|---|---|---|---|
| Volcano | Agua. | Agua. | Agua. | Agua. | Agua. | Agua. | Agua. | Agua. | Agua. | Agua. | Agua. |
| Major elements (wt%) | | | | | | | | | | | |
| $SiO_2$ | 59.61 | 59.29 | 55.39 | 56.21 | 64.10 | 54.39 | 55.46 | 52.50 | 59.81 | 56.31 | 56.07 |
| $TiO_2$ | 0.75 | 0.76 | 0.84 | 1.02 | 0.65 | 1.03 | 0.83 | 1.12 | 0.75 | 0.91 | 0.91 |
| $Al_2O_3$ | 17.45 | 18.04 | 19.77 | 18.11 | 17.60 | 18.29 | 19.65 | 19.03 | 17.52 | 18.45 | 18.71 |
| FeO | 6.48 | 6.41 | 7.23 | 7.97 | 4.54 | 8.69 | 7.36 | 8.98 | 6.40 | 7.73 | 8.21 |
| MnO | 0.13 | 0.13 | 0.14 | 0.14 | 0.13 | 0.16 | 0.13 | 0.15 | 0.13 | 0.14 | 0.16 |
| MgO | 3.15 | 3.15 | 3.09 | 3.42 | 1.49 | 4.18 | 3.23 | 4.52 | 3.08 | 3.47 | 3.52 |
| CaO | 6.23 | 6.17 | 8.15 | 7.36 | 4.07 | 8.06 | 7.96 | 8.97 | 6.11 | 7.28 | 7.02 |
| $Na_2O$ | 3.99 | 3.92 | 3.87 | 3.80 | 4.58 | 3.81 | 3.81 | 3.45 | 4.00 | 3.88 | 3.51 |
| $K_2O$ | 1.99 | 1.90 | 1.29 | 1.74 | 2.57 | 1.15 | 1.34 | 1.06 | 1.97 | 1.60 | 1.65 |
| $P_2O_5$ | 0.23 | 0.22 | 0.22 | 0.23 | 0.27 | 0.22 | 0.22 | 0.21 | 0.23 | 0.23 | 0.22 |
| RTotal | 100.00 | 100.00 | 100.00 | 100.00 | 100.00 | 100.00 | 100.00 | 100.00 | 100.00 | 100.00 | 100.00 |
| Sum | 97.72 | 97.99 | 98.63 | 98.35 | 97.88 | 98.34 | 98.56 | 98.28 | 98.81 | 98.76 | 97.96 |

| Sample | GAG.13A | GAG.13B | GAG.14A | GAG.14B | GAG.15 | GAG.16 | GAG.17 | GAG.18 | GAG.19 | GAG.20 | GAG.21 |
|---|---|---|---|---|---|---|---|---|---|---|---|
| Volcano | Agua. | Agua. | Agua. | Agua. | Agua. | Agua. | Agua. | Agua. | Agua. | Agua. | Agua. |
| Major elements (wt%) | | | | | | | | | | | |
| $SiO_2$ | 69.81 | 59.00 | 52.31 | 52.58 | 55.13 | 58.78 | 54.03 | 55.75 | 53.24 | 54.00 | 52.53 |
| $TiO_2$ | 0.42 | 0.93 | 1.07 | 1.09 | 1.03 | 0.87 | 0.82 | 0.89 | 0.95 | 0.93 | 0.96 |
| $Al_2O_3$ | 15.86 | 17.88 | 18.93 | 18.84 | 19.48 | 18.16 | 19.94 | 18.17 | 19.22 | 18.83 | 19.77 |
| FeO | 2.43 | 6.84 | 8.99 | 8.99 | 7.79 | 6.59 | 7.77 | 8.12 | 8.58 | 8.39 | 8.74 |
| MnO | 0.09 | 0.14 | 0.15 | 0.15 | 0.15 | 0.14 | 0.14 | 0.15 | 0.15 | 0.14 | 0.15 |
| MgO | 0.78 | 2.69 | 4.73 | 4.78 | 2.99 | 2.67 | 3.75 | 4.03 | 4.62 | 4.52 | 4.61 |
| CaO | 2.29 | 5.94 | 9.15 | 8.82 | 7.84 | 6.20 | 8.61 | 7.51 | 8.52 | 8.23 | 8.67 |
| $Na_2O$ | 4.52 | 4.48 | 3.41 | 3.46 | 3.96 | 4.35 | 3.61 | 3.80 | 3.45 | 3.55 | 3.44 |
| $K_2O$ | 3.71 | 1.83 | 1.06 | 1.08 | 1.39 | 1.93 | 1.16 | 1.36 | 1.05 | 1.21 | 0.92 |
| $P_2O_5$ | 0.09 | 0.27 | 0.20 | 0.21 | 0.23 | 0.29 | 0.17 | 0.20 | 0.20 | 0.20 | 0.20 |
| RTotal | 100.00 | 100.00 | 100.00 | 100.00 | 100.00 | 100.00 | 100.00 | 100.00 | 100.00 | 100.00 | 100.00 |
| Sum | 98.02 | 98.28 | 98.47 | 98.05 | 98.71 | 98.41 | 98.19 | 98.36 | 98.00 | 97.83 | 97.84 |

| Sample | GAG.22 | GAG.23 | GAG.24 | GAG.25 | GAG.26 | GAG.27 | GAG.28 | GAG.29 | GAG.30 | GAG.31 | GAG.32 |
|---|---|---|---|---|---|---|---|---|---|---|---|
| Volcano | Agua. | Agua. | Agua. | Agua. | Agua. | Agua. | Agua. | Agua. | Agua | Agua. | Agua |
| Major elements (wt%) | | | | | | | | | | | |
| $SiO_2$ | 53.17 | 54.58 | 58.85 | 59.55 | 55.47 | 56.05 | 55.20 | 53.86 | 58.75 | 58.64 | 53.33 |
| $TiO_2$ | 0.95 | 0.92 | 0.92 | 0.81 | 0.85 | 0.84 | 0.89 | 1.00 | 0.92 | 0.94 | 1.00 |
| $Al_2O_3$ | 18.72 | 18.69 | 17.70 | 18.83 | 20.58 | 20.09 | 20.13 | 18.68 | 17.86 | 18.10 | 18.92 |
| FeO | 8.69 | 8.25 | 6.96 | 5.80 | 6.69 | 6.71 | 7.13 | 8.44 | 6.92 | 7.00 | 8.79 |
| MnO | 0.15 | 0.15 | 0.15 | 0.13 | 0.12 | 0.13 | 0.13 | 0.15 | 0.14 | 0.13 | 0.15 |
| MgO | 4.85 | 4.29 | 2.93 | 2.08 | 2.69 | 2.71 | 2.94 | 4.48 | 2.76 | 2.65 | 4.46 |
| CaO | 8.76 | 7.98 | 6.20 | 6.08 | 8.01 | 7.69 | 8.06 | 8.45 | 6.09 | 6.06 | 8.36 |
| $Na_2O$ | 3.50 | 3.68 | 4.14 | 4.48 | 4.12 | 4.01 | 4.05 | 3.54 | 4.46 | 4.42 | 3.65 |
| $K_2O$ | 1.03 | 1.26 | 1.92 | 1.96 | 1.26 | 1.55 | 1.24 | 1.20 | 1.83 | 1.78 | 1.14 |
| $P_2O_5$ | 0.18 | 0.21 | 0.21 | 0.28 | 0.22 | 0.22 | 0.22 | 0.19 | 0.27 | 0.27 | 0.20 |
| RTotal | 100.00 | 100.00 | 100.00 | 100.00 | 100.00 | 100.00 | 100.00 | 100.00 | 100.00 | 100.00 | 100.00 |
| Sum | 98.29 | 98.67 | 98.51 | 98.91 | 99.28 | 98.68 | 98.17 | 98.12 | 98.62 | 98.27 | 98.33 |

Table 1 (*Continued*).

| Sample | GAG.33 | GAG.34 | GAG.35 | GAG.36 | GPA.01 | GPA.02 | GPA.03 | GPA.04 | GPA.05 | GPA.06 |
|---|---|---|---|---|---|---|---|---|---|---|
| Volcano | Agua. | Agua. | Agua. | Agua. | Pac. | Pac. | Pac. | Pac. | Pac. | Pac. |
| Major elements (wt%) | | | | | | | | | | |
| $SiO_2$ | 57.48 | 58.34 | 54.58 | 53.76 | 50.06 | 51.13 | 50.74 | 51.59 | 50.90 | 51.16 |
| $TiO_2$ | 0.87 | 0.93 | 0.92 | 1.02 | 1.09 | 1.10 | 1.12 | 1.14 | 1.06 | 1.16 |
| $Al_2O_3$ | 18.57 | 18.09 | 19.64 | 18.65 | 20.92 | 20.53 | 20.31 | 19.79 | 21.10 | 20.16 |
| FeO | 6.94 | 7.04 | 7.81 | 8.76 | 8.94 | 8.89 | 9.11 | 8.98 | 8.46 | 9.03 |
| MnO | 0.14 | 0.14 | 0.14 | 0.16 | 0.15 | 0.16 | 0.16 | 0.16 | 0.15 | 0.16 |
| MgO | 3.00 | 2.77 | 3.43 | 4.38 | 3.98 | 3.78 | 3.74 | 4.03 | 3.26 | 3.56 |
| CaO | 6.85 | 6.25 | 8.13 | 8.27 | 10.68 | 9.89 | 10.39 | 9.65 | 10.62 | 10.17 |
| $Na_2O$ | 4.15 | 4.39 | 3.83 | 3.55 | 3.27 | 3.47 | 3.39 | 3.56 | 3.45 | 3.51 |
| $K_2O$ | 1.72 | 1.77 | 1.28 | 1.24 | 0.70 | 0.82 | 0.81 | 0.86 | 0.77 | 0.84 |
| $P_2O_5$ | 0.26 | 0.27 | 0.23 | 0.20 | 0.20 | 0.22 | 0.23 | 0.23 | 0.22 | 0.24 |
| RTotal | 100.00 | 100.00 | 100.00 | 100.00 | 100.00 | 100.00 | 100.00 | 100.00 | 100.00 | 100.00 |
| Sum | 98.52 | 98.49 | 98.59 | 98.07 | 98.88 | 98.49 | 98.47 | 98.44 | 98.72 | 98.48 |

| Sample | GPA.07 | QTAP.1 | QTAP.2 | QTAP.3 | QTAP.4 | QTAP.5 | QTAP.6 | QAS.7 | QAS.8 | QAS.9 |
|---|---|---|---|---|---|---|---|---|---|---|
| Volcano | Pac. | Tec. | Tec. | Tec. | Tec. | Pac. | Pac. | Pac. | Pac. | Tec. |
| Major elements (wt%) | | | | | | | | | | |
| $SiO_2$ | 51.06 | 54.75 | 58.77 | 59.82 | 58.04 | 53.09 | 57.65 | 61.22 | 59.50 | 57.15 |
| $TiO_2$ | 1.13 | 0.88 | 0.74 | 0.71 | 0.68 | 0.93 | 0.92 | 0.63 | 0.67 | 0.76 |
| $Al_2O_3$ | 20.42 | 18.80 | 18.13 | 18.22 | 17.65 | 18.81 | 17.94 | 17.31 | 17.41 | 17.95 |
| FeO | 8.91 | 8.55 | 7.15 | 6.60 | 7.78 | 8.87 | 7.73 | 6.29 | 6.77 | 7.54 |
| MnO | 0.15 | 0.16 | 0.16 | 0.12 | 0.21 | 0.17 | 0.19 | 0.13 | 0.15 | 0.14 |
| MgO | 3.43 | 4.14 | 2.88 | 3.16 | 3.21 | 3.96 | 3.01 | 2.72 | 3.18 | 3.61 |
| CaO | 10.30 | 8.27 | 6.62 | 5.93 | 7.58 | 9.73 | 6.97 | 6.15 | 7.01 | 8.11 |
| $Na_2O$ | 3.52 | 3.32 | 3.71 | 3.44 | 3.83 | 3.39 | 4.04 | 3.68 | 3.59 | 3.33 |
| $K_2O$ | 0.83 | 0.97 | 1.65 | 1.85 | 0.83 | 0.86 | 1.33 | 1.74 | 1.62 | 1.31 |
| $P_2O_5$ | 0.24 | 0.16 | 0.20 | 0.15 | 0.17 | 0.17 | 0.22 | 0.12 | 0.12 | 0.10 |
| RTotal | 100.00 | 100.00 | 100.00 | 100.00 | 100.00 | 100.00 | 100.00 | 100.00 | 100.00 | 100.00 |
| Sum | 98.82 | 97.08 | 96.32 | 96.39 | 94.94 | 92.07 | 96.06 | 96.47 | 94.72 | 92.16 |

| Sample | IXH.10 | IXH.11 | QAM.12 | QAM.13 | QAM.14 | QAM.15 | IXH.16 | IXH.17 | IXH.19 | IXH.20 |
|---|---|---|---|---|---|---|---|---|---|---|
| Volcano | Tec. | Tec. | Tec. | Tec. | Tec. | Tec. | Tec. | Tec. | Tec. | Tec. |
| Major elements (wt%) | | | | | | | | | | |
| $SiO_2$ | 53.59 | 53.35 | 54.60 | 53.20 | 54.92 | 52.48 | 52.28 | 59.12 | 57.58 | 60.30 |
| $TiO_2$ | 0.99 | 1.05 | 0.81 | 0.85 | 0.89 | 0.89 | 0.90 | 0.72 | 0.71 | 0.62 |
| $Al_2O_3$ | 18.93 | 18.66 | 18.54 | 18.35 | 18.29 | 18.21 | 18.62 | 20.33 | 18.14 | 19.59 |
| FeO | 8.37 | 9.03 | 8.45 | 9.38 | 8.52 | 9.50 | 9.27 | 4.98 | 7.58 | 4.80 |
| MnO | 0.13 | 0.15 | 0.17 | 0.20 | 0.25 | 0.18 | 0.14 | 0.10 | 0.17 | 0.12 |
| MgO | 4.53 | 4.37 | 3.98 | 4.20 | 3.95 | 5.49 | 5.50 | 1.50 | 3.38 | 1.46 |
| CaO | 8.98 | 8.61 | 8.79 | 9.26 | 8.48 | 8.95 | 9.26 | 6.85 | 7.06 | 6.47 |
| $Na_2O$ | 3.08 | 3.49 | 3.81 | 3.57 | 3.65 | 3.40 | 3.18 | 3.72 | 3.81 | 4.07 |
| $K_2O$ | 1.26 | 1.11 | 0.71 | 0.82 | 0.88 | 0.73 | 0.69 | 2.40 | 1.40 | 2.36 |
| $P_2O_5$ | 0.14 | 0.17 | 0.15 | 0.16 | 0.17 | 0.18 | 0.15 | 0.28 | 0.17 | 0.21 |
| RTotal | 100.00 | 100.00 | 100.00 | 100.00 | 100.00 | 100.00 | 100.00 | 100.00 | 100.00 | 100.00 |
| Sum | 97.12 | 96.01 | 94.78 | 93.62 | 96.39 | 96.31 | 97.27 | 96.05 | 93.80 | 94.50 |

Table 1 (*Continued*).

| Sample | QTAPG.21 | QTAPG.22 | QTAPG.23 | QTAPG.24 | T.301 | T.302 | M.5 | M.201 | M.202 | M.203 |
|---|---|---|---|---|---|---|---|---|---|---|
| Volcano | Tec. | Tec. | Tec. | Tec. | Tec. | Tec. | Moy. | Moy. | Moy. | Moy. |
| Major elements (wt%) | | | | | | | | | | |
| $SiO_2$ | 61.14 | 58.06 | 60.31 | 60.26 | 53.63 | 53.53 | 66.95 | 58.39 | 57.55 | 56.91 |
| $TiO_2$ | 0.65 | 0.74 | 0.68 | 0.66 | 0.79 | 0.77 | 0.55 | 0.79 | 0.82 | 0.84 |
| $Al_2O_3$ | 17.56 | 17.76 | 17.50 | 17.24 | 18.75 | 18.02 | 16.32 | 17.28 | 18.84 | 18.93 |
| FeO | 6.18 | 7.34 | 6.52 | 6.43 | 8.46 | 8.12 | 3.98 | 7.76 | 7.25 | 7.67 |
| MnO | 0.12 | 0.16 | 0.15 | 0.14 | 0.17 | 0.15 | 0.11 | 0.16 | 0.14 | 0.17 |
| MgO | 2.83 | 3.68 | 3.04 | 3.06 | 5.09 | 5.81 | 0.98 | 3.24 | 2.45 | 2.58 |
| CaO | 6.06 | 7.10 | 6.32 | 6.47 | 8.92 | 9.25 | 3.36 | 6.78 | 7.18 | 7.29 |
| $Na_2O$ | 3.22 | 3.35 | 3.47 | 3.62 | 3.46 | 3.55 | 4.58 | 3.70 | 4.05 | 3.98 |
| $K_2O$ | 2.10 | 1.69 | 1.90 | 1.99 | 0.59 | 0.65 | 3.01 | 1.74 | 1.47 | 1.39 |
| $P_2O_5$ | 0.12 | 0.13 | 0.13 | 0.13 | 0.14 | 0.15 | 0.15 | 0.18 | 0.25 | 0.25 |
| RTotal | 100.00 | 100.00 | 100.00 | 100.00 | 100.00 | 100.00 | 100.00 | 100.00 | 100.00 | 100.00 |
| Sum | 96.53 | 95.80 | 95.48 | 94.41 | 96.90 | 94.88 | 96.00 | 96.05 | 97.36 | 96.53 |

| Sample | M.204 | M.205 | M.206 | M.207 | M.208 | M.209 | M.210 | M.211 | M.212 | TCB.302 |
|---|---|---|---|---|---|---|---|---|---|---|
| Volcano | Moy. | Moy. | Moy. | Moy. | Moy. | Moy. | Moy. | Moy. | Moy. | Tec. |
| Major elements (wt%) | | | | | | | | | | |
| $SiO_2$ | 59.07 | 57.35 | 58.97 | 54.96 | 51.04 | 56.18 | 61.38 | 56.91 | 59.07 | 54.74 |
| $TiO_2$ | 0.76 | 0.79 | 0.71 | 0.77 | 0.79 | 0.64 | 0.68 | 0.84 | 0.76 | 0.75 |
| $Al_2O_3$ | 16.96 | 17.81 | 17.58 | 18.75 | 19.38 | 20.43 | 17.61 | 18.93 | 16.96 | 18.24 |
| FeO | 7.17 | 7.62 | 7.13 | 8.13 | 9.30 | 6.31 | 6.03 | 7.67 | 7.17 | 7.64 |
| MnO | 0.17 | 0.16 | 0.16 | 0.18 | 0.16 | 0.11 | 0.10 | 0.17 | 0.17 | 0.14 |
| MgO | 2.98 | 3.62 | 2.77 | 3.93 | 5.14 | 2.48 | 2.35 | 2.58 | 2.98 | 5.52 |
| CaO | 6.63 | 7.17 | 6.73 | 8.43 | 10.47 | 8.64 | 6.04 | 7.29 | 6.63 | 8.73 |
| $Na_2O$ | 3.94 | 3.60 | 4.24 | 3.64 | 2.90 | 3.85 | 4.02 | 3.98 | 3.94 | 3.44 |
| $K_2O$ | 2.12 | 1.74 | 1.56 | 1.06 | 0.67 | 1.23 | 1.64 | 1.39 | 2.12 | 0.63 |
| $P_2O_5$ | 0.20 | 0.16 | 0.16 | 0.15 | 0.13 | 0.13 | 0.15 | 0.25 | 0.20 | 0.15 |
| RTotal | 100.00 | 100.00 | 100.00 | 100.00 | 100.00 | 100.00 | 100.00 | 100.00 | 100.00 | 100.00 |
| Sum | 94.28 | 96.65 | 93.58 | 95.50 | 97.00 | 93.50 | 95.64 | 94.89 | 96.17 | 98.40 |

RTotal = recalculated total, sum = XRF total before recalculating to 100%.

mafic composition (Bardintzeff and Deniel, 1992). Structurally, Pacaya lies on the actively deforming Chortis microblock at the junction of the Mixto and the dextral Jalpatagua faults (Burkhart and Self, 1985).

Tecuamburro and Moyuta have received attention as geothermal energy prospects (Duffield et al., 1992; Goff et al., 1991). Tecuamburro lies within the south-central part of an approximately 20-km-wide graben that terminates in the north against the Jalpatagua strike–slip fault (Duffield et al., 1992). The Tecuamburro graben has played host to numerous episodes of volcanic activity. The oldest radiometric age of 2.6 Ma was determined on andesitic rocks from the graben's northwest margin (Duffield et al., 1992). Tecuamburro and its summit domes were constructed within a crater formed by sector collapse dated at 38.3 ka based on age dates of associated pyroclastic deposits (Duffield et al., 1992). Lavas from monogenetic cinder cones just north of the graben overlie Tecuamburro rocks and likely represent the youngest magmatic products in the area. Moyuta lies in the extreme southeast corner of Guatemala and consists of a late Quaternary andesitic stratovolcano with associated dacitic domes.

## 3. Samples and preparation

A total of 79 new samples were collected at the four stratovolcanoes for this geochemical study. Twenty-five samples were taken at Volcán Tecuamburro using the Los Alamos geologic base

Table 2
Trace element chemistry of lavas from VF stratovolcanoes

| Sample<br>Volcano | GAG.09<br>Agua.MSU | GAG.10<br>Agua.ND | GAG.13A<br>Agua.ND | GAG.14A<br>Agua.MSU | GAG.19<br>Agua.MSU | GAG.21<br>Agua.ND | GAG.22<br>Agua.MSU | GAG.27<br>Agua.ND | GAG.36<br>Aqua.MSU | GPA.01<br>Pac.ND |
|---|---|---|---|---|---|---|---|---|---|---|
| Trace elements (ppm) | | | | | | | | | | |
| Rb[a] | 19.2 | 48.8 | 97.7 | 20.8 | 20.6 | 15.9 | 20.6 | 31.9 | 29.4 | 9.3 |
| Zr[a] | 94.3 | 161.3 | 243.7 | 92.5 | 102.5 | 102.3 | 90.0 | 128.5 | 109.3 | 71.8 |
| Sr[a] | 588.7 | 528.3 | 247.9 | 595.8 | 567.7 | 576.8 | 551.0 | 571.8 | 561.4 | 632.4 |
| Sc[a] | 27.2 | 12.6 | 6.2 | 25.5 | 25.1 | 20.7 | 23.1 | 17.2 | 23.8 | 25.6 |
| Y[b] | 21.03 | 19.69 | 18.85 | 20.26 | 20.20 | 19.59 | 18.50 | 23.80 | 20.58 | 16.96 |
| Ba[b] | 448.91 | 748.69 | 1100.11 | 446.98 | 493.45 | 519.95 | 419.27 | 638.14 | 489.70 | 341.17 |
| La[b] | 9.29 | 16.09 | 21.29 | 9.15 | 10.19 | 10.48 | 8.60 | 13.19 | 10.75 | 8.20 |
| Ce[b] | 22.21 | 35.98 | 44.91 | 21.45 | 23.47 | 24.68 | 20.50 | 29.95 | 24.48 | 19.34 |
| Pr[b] | 3.14 | 4.98 | 5.34 | 3.00 | 3.24 | 3.56 | 2.84 | 4.41 | 3.46 | 2.85 |
| Nd[b] | 14.48 | 20.43 | 19.14 | 13.89 | 14.50 | 15.21 | 13.23 | 18.44 | 15.25 | 13.23 |
| Sm[b] | 3.90 | 4.38 | 3.66 | 3.55 | 3.61 | 3.70 | 3.43 | 4.41 | 3.78 | 3.10 |
| Eu[b] | 1.21 | 1.10 | 0.64 | 1.14 | 1.15 | 1.05 | 1.06 | 1.26 | 1.18 | 1.12 |
| Gd[b] | 3.62 | 4.70 | 3.80 | 3.36 | 3.57 | 4.21 | 3.27 | 5.09 | 3.60 | 3.89 |
| Tb[b] | 0.62 | 0.65 | 0.52 | 0.56 | 0.56 | 0.59 | 0.55 | 0.75 | 0.60 | 0.61 |
| Dy[b] | 3.54 | 3.73 | 3.36 | 3.40 | 3.48 | 3.61 | 3.10 | 4.35 | 3.48 | 3.41 |
| Ho[b] | 0.68 | 0.80 | 0.73 | 0.67 | 0.65 | 0.75 | 0.61 | 0.94 | 0.69 | 0.70 |
| Er[b] | 2.02 | 2.24 | 2.22 | 1.84 | 1.87 | 2.11 | 1.72 | 2.53 | 1.96 | 1.94 |
| Yb[b] | 1.89 | 2.08 | 2.47 | 1.80 | 1.77 | 1.93 | 1.76 | 2.43 | 1.95 | 1.81 |
| Lu[b] | 0.29 | 0.36 | 0.39 | 0.29 | 0.29 | 0.29 | 0.26 | 0.38 | 0.30 | 0.26 |
| Nb[b] | 3.10 | 4.61 | 5.98 | 3.16 | 3.48 | 3.09 | 3.06 | 3.78 | 3.46 | 2.65 |
| Hf[b] | 2.48 | 4.65 | 4.50 | 2.41 | 2.70 | 2.96 | 2.37 | 3.78 | 2.70 | 1.98 |
| Ta[b] | 0.26 | 0.36 | 0.46 | 0.28 | 0.25 | 0.16 | 0.26 | 0.25 | 0.31 | 0.15 |
| Pb[b] | 6.13 | 8.12 | 14.22 | 5.58 | 6.34 | 5.49 | 7.51 | 5.07 | 6.32 | 3.26 |
| Th[b] | 1.31 | 3.17 | 7.12 | 1.50 | 1.58 | 1.57 | 1.22 | 2.21 | 1.73 | 0.96 |
| U[b] | 0.59 | 1.46 | 3.05 | 0.63 | 0.65 | 0.67 | 0.52 | 0.99 | 0.73 | 0.42 |
| $^{87}Sr/^{86}Sr$ | . | . | . | . | . | . | . | . | . | . |

| Sample<br>Volcano | GPA.02<br>Pac.MSU | GPA.04<br>Pac.MSU | GPA.06<br>Pac.MSU | GPA.07<br>Pac.MSU | QTAP.1<br>Tec.MSU | QTAP.2<br>Tec.MSU | QTAP.3<br>Tec.MSU | QTAP.4<br>Tec.MSU | QTAP.5<br>Tec.MSU | QTAP.62<br>Tec.MSU |
|---|---|---|---|---|---|---|---|---|---|---|
| Trace elements (ppm) | | | | | | | | | | |
| Rb[b] | 13.5 | 13.0 | 13.3 | 12.9 | 18.7 | 32.9 | 39.5 | 13.3 | 11.6 | 25.1 |
| Zr[b] | 80.1 | 81.1 | 85.4 | 81.8 | 78.0 | 105.4 | 122.9 | 76.9 | 65.8 | 99.7 |
| Sr[b] | 639.6 | 585.4 | 622.6 | 635.6 | 497.8 | 467.7 | 376.5 | 414.5 | 456.5 | 437.0 |
| Sc[b] | 28.8 | 25.6 | 29.1 | 23.5 | 18.8 | 11.5 | 16.8 | 15.1 | 24.2 | 21.1 |
| Y[b] | 18.64 | 21.71 | 21.04 | 20.26 | 27.49 | 29.25 | 44.30 | 20.15 | 18.20 | 81.83 |
| Ba[b] | 427.67 | 451.08 | 419.18 | 420.50 | 418.01 | 610.10 | 750.89 | 424.40 | 338.33 | 622.21 |
| La[b] | 9.36 | 9.08 | 9.89 | 10.13 | 9.03 | 10.73 | 19.11 | 6.10 | 5.28 | 23.10 |
| Ce[b] | 21.45 | 20.47 | 22.04 | 22.87 | 14.95 | 20.54 | 21.16 | 14.17 | 11.91 | 23.19 |
| Pr[b] | 2.96 | 2.88 | 3.19 | 3.28 | 2.79 | 3.32 | 5.05 | 2.30 | 2.04 | 6.87 |
| Nd[b] | 13.67 | 13.64 | 14.48 | 15.21 | 13.44 | 14.80 | 21.60 | 10.78 | 9.83 | 31.99 |
| Sm[b] | 3.50 | 3.77 | 3.70 | 4.19 | 3.22 | 3.58 | 5.08 | 2.87 | 2.62 | 7.84 |
| Eu[b] | 1.23 | 1.21 | 1.28 | 1.32 | 1.04 | 1.11 | 1.54 | 0.93 | 0.88 | 2.48 |
| Gd[b] | 3.45 | 3.52 | 3.36 | 3.70 | 3.52 | 3.79 | 5.23 | 3.04 | 2.76 | 9.02 |
| Tb[b] | 0.55 | 0.60 | 0.59 | 0.61 | 0.58 | 0.62 | 0.88 | 0.50 | 0.46 | 1.54 |
| Dy[b] | 3.08 | 3.65 | 3.63 | 3.54 | 3.86 | 3.77 | 5.51 | 3.16 | 2.94 | 9.57 |
| Ho[b] | 0.62 | 0.72 | 0.69 | 0.71 | 0.79 | 0.79 | 1.19 | 0.65 | 0.61 | 2.01 |
| Er[b] | 1.73 | 2.02 | 1.98 | 2.04 | 2.37 | 2.36 | 3.45 | 1.97 | 1.86 | 5.95 |
| Yb[b] | 1.76 | 1.86 | 1.77 | 2.00 | 2.10 | 2.28 | 3.30 | 2.04 | 1.83 | 5.67 |
| Lu[b] | 0.26 | 0.31 | 0.26 | 0.28 | 0.33 | 0.37 | 0.51 | 0.33 | 0.29 | 0.92 |
| Nb[b] | 3.40 | 3.36 | 3.41 | 3.46 | 2.15 | 3.04 | 3.47 | 2.71 | 2.12 | 2.73 |
| Hf[b] | 1.88 | 2.14 | 2.05 | 2.18 | 2.08 | 2.96 | 3.15 | 2.32 | 2.01 | 2.50 |
| Ta[b] | 0.26 | 0.27 | 0.27 | 0.28 | 0.14 | 0.21 | 0.27 | 0.18 | 0.13 | 0.17 |

Table 2 (*Continued*).

| Sample | GPA.02 | GPA.04 | GPA.06 | GPA.07 | QTAP.1 | QTAP.2 | QTAP.3 | QTAP.4 | QTAP.5 | QTAP.62 |
|---|---|---|---|---|---|---|---|---|---|---|
| Volcano | Pac.MSU | Pac.MSU | Pac.MSU | Pac.MSU | Tec.MSU | Tec.MSU | Tec.MSU | Tec.MSU | Tec.MSU | Tec.MSU |
| Pb[b] | 4.97 | 4.45 | 4.97 | 5.52 | 3.46 | 5.72 | 5.49 | 3.66 | 2.89 | 5.09 |
| Th[b] | 1.19 | 1.09 | 1.22 | 1.21 | 1.49 | 2.26 | 2.42 | 0.72 | 0.68 | 1.39 |
| U[b] | 0.53 | 0.49 | 0.53 | 0.53 | 0.62 | 0.85 | 1.29 | 0.36 | 0.32 | 0.72 |
| $^{87}Sr/^{86}Sr$ | . | . | . | . | 0.70377 | . | 0.70379 | 0.70372 | . | 0.70380 |

| Sample | QAS.7 | QAS.8 | QAS.9 | IXH.10 | IXH.11 | QAM.12 | QAM.13 | QAM.14 | QAM.15 | IXH.16 | IXH.17 |
|---|---|---|---|---|---|---|---|---|---|---|---|
| Volcano | Tec.MSU | Tec.MSU | Tec.MSU | Tec.MSU | Tec.MSU | Tec.MSU | Tec.MSU | Tec.MSU | Tec.MSU | Tec.MSU | Tec.MSU |
| Trace elements (ppm) | | | | | | | | | | | |
| Rb[a] | 35.0 | 28.3 | 22.0 | 29.2 | 20.7 | 8.4 | 12.6 | 13.1 | 10.0 | 13.0 | 50.3 |
| Zr[a] | 110.4 | 103.4 | 78.2 | 73.0 | 81.9 | 76.9 | 69.0 | 97.9 | 82.4 | 59.5 | 150.2 |
| Sr[a] | 346.3 | 349.9 | 356.9 | 485.5 | 484.0 | 439.2 | 436.4 | 407.0 | 419.6 | 515.2 | 498.0 |
| Sc[a] | 15.5 | 16.0 | 19.1 | 25.6 | 22.0 | 18.1 | 22.6 | 24.9 | 23.3 | 23.9 | 14.0 |
| Y[b] | 27.36 | 21.73 | 19.99 | 18.12 | 17.89 | 20.05 | 21.74 | 35.54 | 20.23 | 24.85 | 51.10 |
| Ba[b] | 608.64 | 566.18 | 469.88 | 419.32 | 425.74 | 346.05 | 471.30 | 371.94 | 311.66 | 323.77 | 716.54 |
| La[b] | 9.36 | 7.68 | 5.67 | 7.47 | 7.73 | 5.40 | 7.24 | 6.66 | 5.70 | 8.74 | 29.79 |
| Ce[b] | 17.04 | 16.38 | 12.19 | 14.86 | 15.69 | 11.98 | 14.78 | 14.40 | 13.49 | 12.29 | 33.86 |
| Pr[b] | 2.76 | 2.43 | 1.84 | 2.51 | 2.78 | 2.00 | 2.35 | 2.39 | 2.14 | 3.53 | 10.47 |
| Nd[b] | 12.10 | 12.75 | 11.16 | 11.49 | 8.90 | 9.07 | 11.47 | 13.03 | 9.85 | 11.09 | 12.07 |
| Sm[b] | 2.86 | 3.19 | 2.48 | 2.95 | 2.16 | 2.48 | 2.95 | 3.38 | 2.43 | 2.68 | 3.08 |
| Eu[b] | 0.87 | 0.95 | 0.77 | 0.87 | 0.71 | 0.78 | 0.98 | 1.08 | 0.82 | 0.92 | 0.95 |
| Gd[b] | 3.11 | 3.57 | 2.67 | 3.09 | 2.40 | 2.71 | 3.06 | 3.32 | 2.70 | 2.88 | 3.46 |
| Tb[b] | 0.54 | 0.60 | 0.46 | 0.51 | 0.39 | 0.45 | 0.53 | 0.55 | 0.45 | 0.49 | 0.59 |
| Dy[b] | 3.89 | 3.78 | 3.10 | 3.20 | 2.79 | 2.90 | 3.10 | 3.21 | 3.13 | 3.44 | 4.30 |
| Ho[b] | 0.81 | 0.79 | 0.65 | 0.67 | 0.60 | 0.62 | 0.63 | 0.63 | 0.66 | 0.69 | 0.91 |
| Er[b] | 2.59 | 2.54 | 1.98 | 2.08 | 1.86 | 1.90 | 1.82 | 1.78 | 1.97 | 2.13 | 2.69 |
| Yb[b] | 2.55 | 2.70 | 1.89 | 2.15 | 1.72 | 1.88 | 1.69 | 1.56 | 1.81 | 2.01 | 2.37 |
| Lu[b] | 0.42 | 0.44 | 0.30 | 0.33 | 0.26 | 0.29 | 0.27 | 0.24 | 0.27 | 0.32 | 0.37 |
| Nb[b] | 2.63 | 2.78 | 2.45 | 2.84 | 1.90 | 2.39 | 2.27 | 2.78 | 1.91 | 1.97 | 2.64 |
| Hf[b] | 2.90 | 3.07 | 2.74 | 2.95 | 2.11 | 2.40 | 2.27 | 2.58 | 1.97 | 1.82 | 2.56 |
| Ta[b] | 0.20 | 0.21 | 0.18 | 0.20 | 0.14 | 0.15 | 0.18 | 0.18 | 0.12 | 0.12 | 0.17 |
| Pb[b] | 5.40 | 4.82 | 5.59 | 5.10 | 4.37 | 4.09 | 4.74 | 4.31 | 3.83 | 4.03 | 4.01 |
| Th[b] | 1.85 | 1.73 | 1.64 | 1.55 | 1.25 | 1.23 | 2.78 | 1.94 | 0.53 | 1.24 | 0.83 |
| U[b] | 0.81 | 0.73 | 0.75 | 0.67 | 0.59 | 0.52 | 0.98 | 0.74 | 0.29 | 0.56 | 0.43 |
| $^{87}Sr/^{86}Sr$ | 0.70370 | 0.70373 | 0.70373 | . | 0.70380 | . | . | 0.70373 | . | . | 0.70377 |

| Sample | IXH.19 | IXH.20 | QPG.21 | QPG.22 | QPG.23 | QPG.24 | QTAI.301 | QTAI.302 | TCB.302 | M.201 | M.202 |
|---|---|---|---|---|---|---|---|---|---|---|---|
| Volcano | Tec.MSU | Tec.MSU | Tec.MSU | Tec.MSU | Tec.MSU | Tec.MSU | Tec.RUT | Tec.RUT | Tec.ND | Moy.MSU | Moy.MSU |
| Trace elements (ppm) | | | | | | | | | | | |
| Rb[a] | 28.0 | 55.1 | 48.1 | 36.5 | 43.1 | 45.8 | 7.4 | 9.6 | 10.1 | 39.3 | 33.4 |
| Zr[a] | 98.3 | 161.9 | 125.0 | 111.5 | 124.3 | 122.5 | 68.3 | 71.7 | 75.4 | 141.1 | 132.5 |
| Sr[a] | 442.3 | 422.2 | 370.9 | 393.6 | 371.7 | 368.8 | 420.0 | 447.0 | 449.0 | 411.9 | 473.7 |
| Sc[a] | 18.5 | 14.3 | 16.5 | 19.9 | 19.2 | 17.0 | 26.9 | 25.6 | 26.9 | 19.0 | 16.5 |
| Y[b] | 53.60 | 25.38 | 52.61 | 29.45 | 39.19 | 21.43 | 17.08 | 24.33 | 14.69 | 29.41 | 40.36 |
| Ba[b] | 662.34 | 777.33 | 729.44 | 753.33 | 708.18 | 681.94 | 311.00 | 289.90 | 314.73 | 692.91 | 666.21 |
| La[b] | 14.19 | 13.98 | 39.83 | 10.80 | 20.63 | 10.64 | 4.37 | 6.95 | 5.83 | 11.52 | 16.94 |
| Ce[b] | 23.86 | 35.16 | 33.56 | 22.07 | 24.92 | 21.86 | 12.24 | 13.59 | 14.07 | 24.06 | 26.72 |
| Pr[b] | 4.37 | 4.47 | 11.72 | 3.28 | 5.90 | 3.22 | 2.35 | 2.93 | 2.07 | 3.89 | 6.27 |
| Nd[b] | 10.62 | 17.70 | 46.32 | 18.69 | 18.07 | 50.32 | 9.03 | 10.57 | 9.45 | 14.28 | 25.16 |
| Sm[b] | 2.74 | 4.94 | 11.19 | 4.86 | 4.40 | 11.12 | 2.46 | 2.67 | 2.35 | 3.51 | 5.76 |
| Eu[b] | 0.87 | 1.76 | 3.10 | 1.57 | 1.24 | 2.78 | 0.86 | 0.94 | 0.80 | 1.02 | 1.56 |
| Gd[b] | 2.87 | 4.84 | 9.71 | 5.00 | 4.14 | 9.89 | 2.67 | 3.00 | 2.92 | 3.54 | 5.72 |
| Tb[b] | 0.45 | 0.78 | 1.61 | 0.94 | 0.65 | 1.63 | 0.45 | 0.49 | 0.48 | 0.63 | 0.96 |
| Dy[b] | 3.29 | 4.64 | 9.49 | 5.99 | 3.94 | 9.29 | 2.74 | 2.92 | 2.82 | 3.86 | 5.98 |

Table 2 (*Continued*).

| Sample<br>Volcano | IXH.19<br>Tec.MSU | IXH.20<br>Tec.MSU | QPG.21<br>Tec.MSU | QPG.22<br>Tec.MSU | QPG.23<br>Tec.MSU | QPG.24<br>Tec.MSU | QTAI.301<br>Tec.RUT | QTAI.302<br>Tec.RUT | TCB.302<br>Tec.ND | M.201<br>Moy.MSU | M.202<br>Moy.MSU |
|---|---|---|---|---|---|---|---|---|---|---|---|
| Ho[b] | 0.66 | 0.86 | 1.77 | 1.33 | 0.80 | 1.70 | 0.58 | 0.62 | 0.59 | 0.79 | 1.16 |
| Er[b] | 2.09 | 2.32 | 4.81 | 3.97 | 2.42 | 4.53 | 1.76 | 1.87 | 1.68 | 2.42 | 3.22 |
| Yb[b] | 1.87 | 2.24 | 4.60 | 3.73 | 2.39 | 4.61 | 1.74 | 1.78 | 1.62 | 2.37 | 3.36 |
| Lu[b] | 0.29 | 0.32 | 0.63 | 0.57 | 0.35 | 0.64 | 0.28 | 0.29 | 0.24 | 0.38 | 0.49 |
| Nb[b] | 2.16 | 2.04 | 4.56 | 2.75 | 5.10 | 3.38 | 2.02 | 2.07 | 2.43 | 3.07 | 3.49 |
| Hf[b] | 2.05 | 1.57 | 4.03 | 2.30 | 3.33 | 3.25 | 2.12 | 2.01 | 2.08 | 2.65 | 3.28 |
| Ta[b] | 0.13 | 0.10 | 0.31 | 0.20 | 0.32 | 0.26 | . | . | 0.14 | 0.21 | 0.26 |
| Pb[b] | 4.31 | 3.21 | 10.08 | 5.65 | 21.83 | 7.51 | 3.49 | 3.95 | 3.27 | 7.30 | 6.90 |
| Th[b] | 0.54 | 0.66 | 3.50 | 1.98 | 2.94 | 2.90 | 0.28 | 0.92 | 0.45 | 2.01 | 2.55 |
| U[b] | 0.29 | 0.35 | 1.76 | 1.07 | 3.06 | 1.43 | 0.22 | 0.21 | 0.25 | 1.05 | 1.30 |
| $^{87}Sr/^{86}Sr$ | 0.70375 | . | . | . | . | 0.70374 | 0.70367 | . | . | . | 0.70372 |

| Sample<br>Volcano | M.203<br>Moy.MSU | M.204<br>Moy.MSU | M.205<br>Moy.MSU | M.206<br>Moy.MSU | M.207<br>Moy.MSU | M.208<br>Moy.MSU | M.209<br>Moy.MSU | M.210<br>Moy.MSU | M.211<br>Moy.MSU | M.212<br>Moy.MSU |
|---|---|---|---|---|---|---|---|---|---|---|
| Trace elements (ppm) | | | | | | | | | | |
| Rb[a] | 28.9 | 47.4 | 38.4 | 29.8 | 20.3 | 11.2 | 17.8 | 32.0 | 24.1 | 28.3 |
| Zr[a] | 129.5 | 169.2 | 143.7 | 106.3 | 76.5 | 54.9 | 76.7 | 140.5 | 113.2 | 125.0 |
| Sr[a] | 475.6 | 392.0 | 413.7 | 417.4 | 446.6 | 483.9 | 456.7 | 397.2 | 408.9 | 420.0 |
| Sc[a] | 19.7 | 17.1 | 18.0 | 15.1 | 21.8 | 30.4 | 15.8 | 15.0 | 19.1 | 17.0 |
| Y[b] | 37.82 | 31.15 | 26.03 | 24.24 | 20.60 | 18.58 | 17.68 | 20.57 | 20.73 | 21.87 |
| Ba[b] | 818.02 | 764.31 | 709.36 | 664.46 | 602.15 | 316.23 | 456.26 | 714.44 | 604.69 | 647.59 |
| La[b] | 14.41 | 13.53 | 10.17 | 9.23 | 6.86 | 5.27 | 5.29 | 8.71 | 7.46 | 8.11 |
| Ce[b] | 28.29 | 28.58 | 22.85 | 18.76 | 15.01 | 11.06 | 12.94 | 19.56 | 15.97 | 18.86 |
| Pr[b] | 5.55 | 4.41 | 3.60 | 3.54 | 2.81 | 1.99 | 2.03 | 3.25 | 2.78 | 2.90 |
| Nd[b] | 13.63 | 17.43 | 28.77 | 24.54 | 19.08 | 15.60 | 15.70 | 13.20 | 9.72 | 9.22 |
| Sm[b] | 3.25 | 4.36 | 7.13 | 6.35 | 4.74 | 3.99 | 4.07 | 3.51 | 2.68 | 2.44 |
| Eu[b] | 0.87 | 1.12 | 1.83 | 1.76 | 1.13 | 1.08 | 1.13 | 1.11 | 0.89 | 0.83 |
| Gd[b] | 3.30 | 4.50 | 6.53 | 6.01 | 4.74 | 3.85 | 3.93 | 3.50 | 2.83 | 2.53 |
| Tb[b] | 0.53 | 0.75 | 1.13 | 0.99 | 0.79 | 0.68 | 0.68 | 0.65 | 0.49 | 0.42 |
| Dy[b] | 3.27 | 4.57 | 6.57 | 6.00 | 4.78 | 4.05 | 4.04 | 3.88 | 3.03 | 2.68 |
| Ho[b] | 0.68 | 0.94 | 1.28 | 1.21 | 0.98 | 0.83 | 0.85 | 0.80 | 0.62 | 0.57 |
| Er[b] | 2.09 | 2.94 | 3.58 | 3.52 | 3.05 | 2.69 | 2.65 | 2.43 | 1.88 | 1.69 |
| Yb[b] | 2.13 | 2.98 | 3.43 | 3.62 | 3.09 | 2.70 | 2.68 | 2.48 | 1.84 | 1.73 |
| Lu[b] | 0.33 | 0.46 | 0.51 | 0.50 | 0.48 | 0.42 | 0.42 | 0.39 | 0.28 | 0.26 |
| Nb[b] | 3.55 | 3.81 | 3.49 | 3.46 | 4.61 | 3.53 | 2.87 | 1.83 | 1.69 | 2.21 |
| Hf[b] | 3.51 | 4.33 | 3.18 | 3.23 | 5.25 | 4.35 | 3.67 | 2.83 | 1.81 | 2.26 |
| Ta[b] | 0.27 | 0.25 | 0.21 | 0.20 | 0.31 | 0.24 | 0.22 | 0.14 | 0.09 | 0.13 |
| Pb[b] | 7.02 | 6.97 | 7.41 | 7.12 | 7.91 | 6.82 | 6.36 | 4.40 | 3.27 | 5.13 |
| Th[b] | 3.28 | 3.57 | 2.55 | 2.63 | 4.23 | 3.55 | 2.37 | 1.82 | 0.98 | 0.97 |
| U[b] | 1.29 | 1.37 | 1.34 | 1.19 | 1.67 | 1.41 | 1.04 | 0.77 | 0.40 | 0.49 |
| $^{87}Sr/^{86}Sr$ | . | 0.70373 | . | 0.70372 | . | . | . | 0.70368 | 0.70363 | 0.70365 |

[a] Trace element measured by XRF.
[b] Trace element measured by ICP-MS.
MSU = Michigan State University; ND = University of Notre Dame; Pac. = Pacaya; Tec. = Tecuamburro; Moy. = Moyuta.

map as a guide (Duffield et al., 1991). The sample suite includes from youngest to oldest: two from the Holocene Tecuamburro volcano vent (Qat unit), four from Miraflores Crater (Qam unit), three from Chupadero crater (Qas unit), four from a central vent in the northern part of the graben (Qtapg unit), six from the Plio–Pleistocene Ixhuatan complex (Qtai unit), and six from a northwestern vent (Qtap unit). An additional 12 samples were collected on a reconnaissance trip to

Volcán Moyuta on the southern boundary of the Jalpatagua graben. Seven fresh basalts of historic eruptions were sampled at Pacaya. The 1775 lava flow was the oldest lava sampled at Pacaya and the youngest was the November 11, 1996 flow. Thirty-five rock samples were taken around the perimeter of Agua. Samples from Agua and Tecuamburro were crushed at Northern Illinois University in a tungsten carbide shatterbox in preparation for X-ray fluorescence (XRF) analyses and an alumina shatterbox for inductively coupled plasma mass spectrometry (ICP-MS) analyses. Tecuamburro and Moyuta lava samples were crushed in alumina at Rutgers University for both XRF and ICP-MS analyses.

## 4. Analytical procedures

Table 1 presents the major element data for all 79 of the samples collected at the VF stratovolcanoes in southeastern Guatemala. Table 2 presents select trace element data for a subset of 52 samples. Major and minor oxides along with select trace elements (Nb, Zr, Y, Sr, Rb, Th, Pb, Ga, Zn, Co, Cr, La, Ba, Sc, and V) were determined by XRF spectrometry on a completely automated Siemens 300 sequential wavelength dispersive system. A low dilution fusion technique using a 2:1 flux-to-sample ratio was adopted for the accurate determination of major, minor, and trace elements in rock samples (Eastell and Willis, 1990). Homogeneous glass fusion discs eliminate particle size effects, and consequently offer a major analytical advantage over the conventional pressed pellet method. The average relative error for the common trace elements was reported at less than 5% and sensitivity decreased by about a factor of two compared with the powder pellet method (Eastell and Willis, 1990).

Trace element and rare earth element (REE) concentrations were determined on a subset of samples using a laser ablation inductively coupled plasma mass spectrometer (LA-ICP-MS; Cetac LSX-200 and Micromass Platform ICP-MS) at Michigan State University. For LA-ICP-MS results, strontium was used as the internal standard and prior to any calculation the background signal was subtracted from standards and samples. The concentrations were calculated based on linear regression techniques using international standards (USGS and Japanese standards). The standards span a wide range of silicate rock compositions, ensuring that unknown samples are within the range of the standards.

For data acquisition, the elements were divided into three groups: light REE (LREE; La–Tb), heavy REE (HREE; Dy–Lu) and other trace elements. Data were acquired for 0.7 min for each group. Before data acquisition, the ICP-MS was optimized while ablating the NIST-612 glass standard. Parameters such as torch position and gas flow rates were adjusted until the maximum and most stable signal was observed for elements with a wide range of masses. For tuning and data acquisition, a signal was considered stable when the instrument response (total ion count) remained above 70% during data acquisition.

A small set of samples were analyzed for trace elements by ICP-MS using a FISONS PlasmaQuad II STE ICP-MS at the University of Notre Dame. Dissolution procedures for rock powders involved HF-$HNO_3$ digestion in screw top teflon beakers. Samples were run in a 2–5% $HNO_3$ matrix with standardization, drift correction, and data reduction following the method of Jenner et al. (1990). At Notre Dame, a more comprehensive 40 element trace element package included all of the REE and Li, Be, Sc, V, Cr, Co, Ni, Cu, Zn, Ga, Rb, Sr, Y, Zr, Nb, Mo, Sn, Sb, Cs, Ba, Hf, Ta, Tl, Pb, Th, and U. Consistency between the LA-ICP-MS analytical technique at Michigan State and the ICP-MS measurements at Notre Dame was within 10% or better.

Sr isotopic ratios were determined on a subset of samples by mass spectrometry on a VG Sector multi-sample, fully automated, thermal ionization mass spectrometer at Rutgers University. Chemical separations for Sr were performed by standard methods of ion-exchange chromatography. Sr isotope ratios are reported as measured, and normalized to $^{86}Sr/^{88}Sr$ of 0.1194. NBS 987 Sr standard is measured at 0.710255 as a long-term average. External reproducibility based on repeated analyses of standards is estimated at better than $\pm 0.000024$ ($2\sigma$ error).

## 5. Results

### 5.1. Major elements

The major element data presented in Table 1 have been recalculated to 100% based on the variability in freshness between the VF stratovolcanoes from the central and southeastern segments. VF lavas from southeastern Guatemala range in composition from basalt to dacite (LeBas et al., 1986). Agua, Tecuamburro, and Moyuta together account for this diversity; Pacaya volcano has erupted exclusively basaltic lavas in historic times. Typical of arc volcanism globally, the vast majority of the samples are basaltic andesite and andesite (Fig. 3a). The VF lavas classify as medium-K andesites (Fig. 3b; Gill, 1981). On a FeO/MgO vs. $SiO_2$ diagram (Fig. 3c), the VF lavas display overall calc-alkaline affinities due to their gentle positive slope despite plotting almost completely in the tholeiitic field (Miyashiro, 1974).

The major element contents of the VF lavas show relatively smooth trends in variation diagrams that use MgO as the measure of differentiation. MgO ranges from 5.81 to 0.78 wt%. $SiO_2$, $Na_2O$, $K_2O$, and $P_2O_5$ increase in concentration with falling MgO content (Fig. 4). $TiO_2$, $Al_2O_3$, FeO, and CaO display a positive correlation with MgO content typical of compatible oxides (Fig. 4). The central segment stratovolcano of Pacaya and to a lesser degree Agua have higher $TiO_2$, $Al_2O_3$, CaO, $Na_2O$, and $P_2O_5$ at a given MgO content than the older stratovolcanoes of the southeast segment. Except for FeO, the modern lavas from Pacaya have similar major element compositions as BVF cinder cones in southeastern Guatemala.

### 5.2. Trace elements

Trace element variation diagrams utilizing MgO as the differentiation index also show coherent trends (Fig. 5). In Fig. 5, only Sc demonstrates a compatible trace element character by virtue of its positive correlation with MgO. Otherwise, the trace elements shown in Fig. 5 all display trends attributed to incompatible trace elements. Except for Nb and Sc, Agua generally has higher incompatible element concentrations at a given MgO value than Pacaya, Tecuamburro, or Moyuta. Tecuamburro and Moyuta display more scatter so that individual samples sometime exceed concentrations of samples from the two younger front volcanoes. REE mobility may be implied by the scatter shown in the La versus MgO diagram (Fig. 5f). We address this issue in more detail in the following section.

## 6. Discussion

### 6.1. REE mobility at Tecuamburro/Moyuta

Post-emplacement changes in the chemical composition of volcanic rocks can lead to erroneous conclusions in petrogenetic models. The recognition in recent years of the complex elemental responses to the varied physico-chemical conditions imposed by weathering and hydrothermal alteration has raised some serious questions about the relative immobility of the REE (Leroy and Turpin, 1988; Marsh, 1991; Price et al., 1991; Kuschel and Smith, 1992; Terakado et al., 1993; Hopf, 1993; Lewis et al., 1997). It is now generally conceded that basalts exposed to hydrothermal activity or weathering even for relatively short periods of time can show significant effects of geochemical alteration (Price et al., 1991). The approach adopted here is to identify those samples affected by secondary processes and remove them from consideration in order to prevent misinterpretations.

Ratios of trace elements with similar degrees of incompatibility in basaltic systems can potentially identify anomalous samples (Price et al., 1991). Young Guatemalan lavas erupted from cinder cones and stratovolcanoes have a fairly constant Nb/Nd ratio (Fig. 6). At a given Nb concentration, there exists a distinct group of samples with elevated Nd abundances that deviate from the trend defined by the other Guatemalan lavas. The anomalous samples include Ixh-16, -17, and -19, Qtapg-21 and -23, Qtap-3 and -6, and GuM-202 and -203. Not only are these samples among the oldest lavas collected for this study, but they also stand out by displaying crossing REE patterns with pronounced Ce anomalies (Cameron, 1998). Thus, higher Nd concentrations in Fig. 6 suggest that REE enrichment accounts for the negative Ce anomalies. Unique among the REE, Ce exists in the 4+ state under oxidizing conditions. The other REE remain in the more soluble 3+ ionic state, and therefore, percolating ground waters mobilize these REE and acquire the REE-enriched pattern with the pronounced negative Ce anomaly. A pH increase or adsorption to clay minerals will cause these ground waters to impart the REE signature to the partly weathered volcanic rocks. These altered samples will be omitted from the petrological diagrams in subsequent sections.

### 6.2. *Differentiation and crustal contamination*

Although andesites are the distinctive rock type at arcs, the primary rock produced by partial melting of the mantle wedge in subduction zones is basalt. Near-primary magma compositions in arcs are exceedingly scarce compared to other tectonic settings. Therefore, arc geochemists have placed greater reliance on melting experiments to help identify the chemical nature of a primary magma in a convergent setting. High-degree experimental partial melts of anhydrous peridotite (e.g. Jacques and Green, 1980; Gaetani and Grove, 1998; Falloon and Danyushevsky, 2000) tend to extend outside the field of primitive arc basalts (Fig. 7). Recent melting experiments have been conducted on peridotite+$H_2O$ mixtures to understand primary magma generation in the arc setting (Kushiro, 1990; Hirose and Kawamoto, 1995; Hirose, 1997; Gaetani and Grove, 1998; Falloon and Danyushevsky, 2000). Rare mafic lavas from island arcs (Kamenetsky et al., 1997; Peate et al., 1997; Hochstaedter et al., 1996a) fall closer to more of the fields occupied by experimental hydrous melts (Fig. 7, inset). Continental arc lavas, in particular, are highly differentiated, often having MgO contents below 5 wt%. Lava samples from Guatemalan stratovolcanoes are no

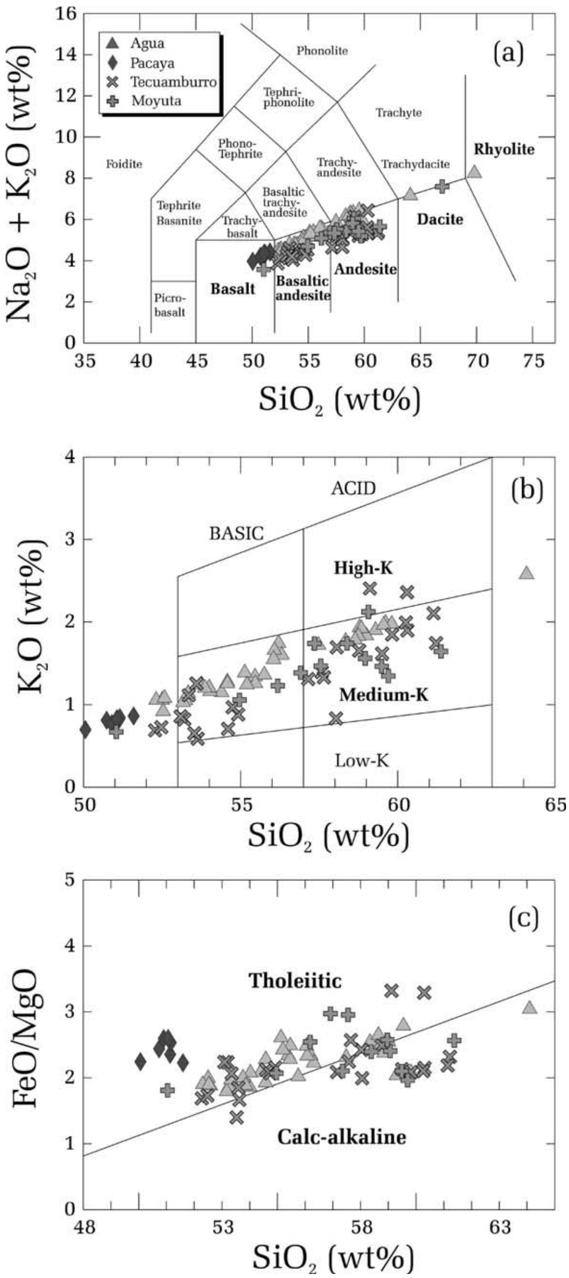


Fig. 3. Major element classification diagrams for the VF lavas. (a) The total alkalis–silica diagram shows that the VF lavas range from basalt to dacite. Modern Pacaya has erupted lavas of uniform basaltic composition. (b) The $K_2O$–$SiO_2$ diagram indicates that the more evolved VF lavas are medium-K andesites and dacites. (c) The VF lavas plot close to the tholeiitic and calc-alkaline dividing line on the FeO/MgO versus $SiO_2$ diagram. Although a majority of the data plot in the tholeiitic field, the near-invariant behavior of FeO/MgO with increasing $SiO_2$ assigns calc-alkaline arc affinities to the VF lavas.

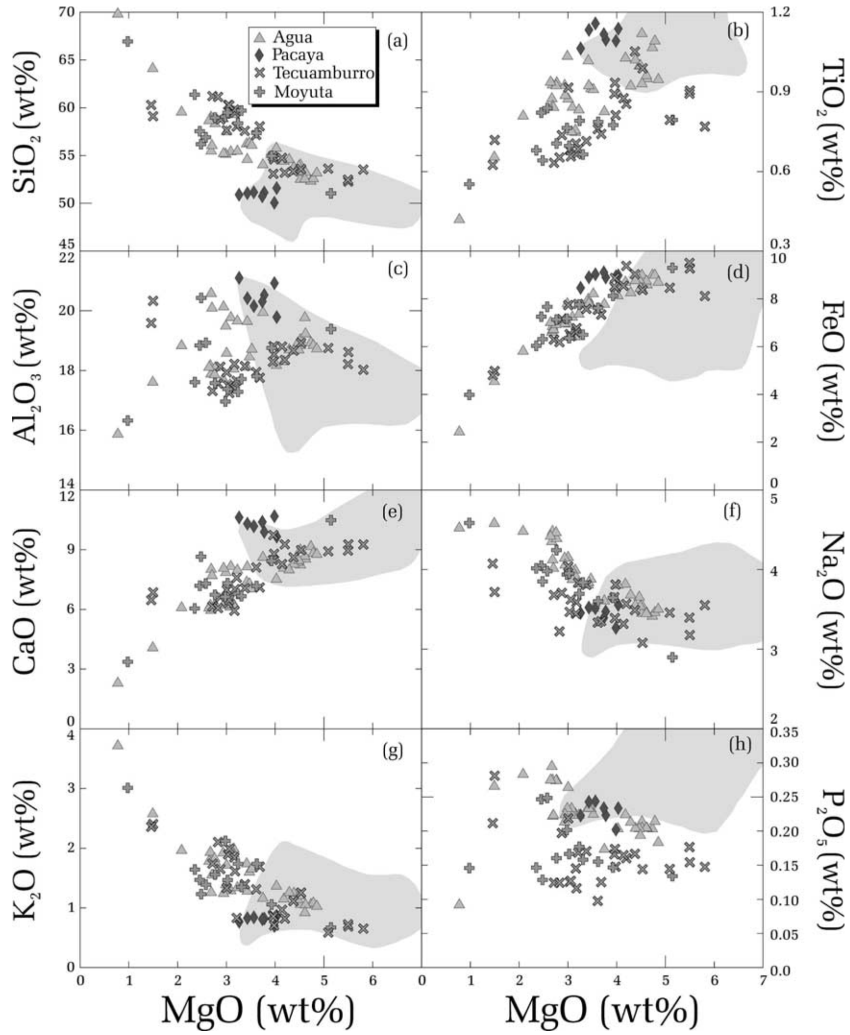


Fig. 4. Major element variation diagrams for the VF lavas from southeastern Guatemala. Major element contents were recalculated to a total of 100%. MgO content on the *x*-axis was adopted as a measure of differentiation. (a) $SiO_2$, (b) $TiO_2$, (c) $Al_2O_3$, (d) FeO, (e) CaO, (f) $Na_2O$, (g) $K_2O$ and (h) $P_2O_5$ versus MgO. The light gray-shaded region shows the field for the BVF cinder cones (Walker et al., 1995, 2000; Cameron, 1998). With the exception of FeO, Pacaya lavas fall close to or within the field for BVF cinder cones in terms of major elements.

exception. The VF lavas plot well to the left of the hydrous melt fields on the CaO–MgO diagram (Fig. 7). This lack of correspondence illustrates the prominent role of differentiation in modifying the arc lavas from southeastern Guatemala.

The trajectory of the VF data on the CaO–MgO diagram will depend on the fractionating assemblage (e.g. Davidson, 1996; Gill, 1981). Near-primary island arc lavas exhibit a gentle negative trend that documents olivine fractionation in the earliest evolutionary stage. The inflection point shown by the primitive island arc data records the change from olivine-dominated to combined olivine–pyroxene–plagioclase fractionation. The steep positive correlation shown by the VF lavas argues for the prominent role of pyroxene and plagioclase in the fractionating assemblage (Fig. 7). Pressure and $H_2O$ content control the relative proportions of these minerals and the onset of each fractionating phase (Grove and

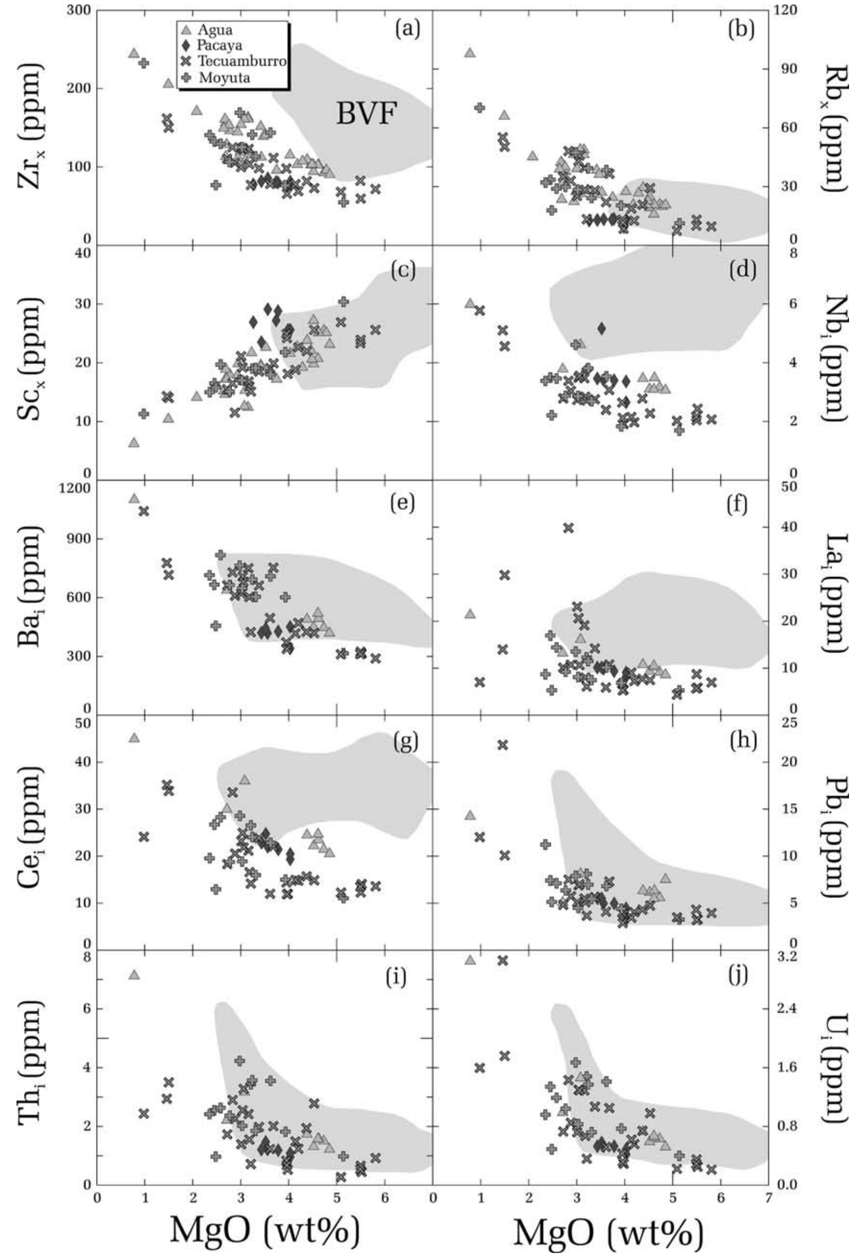


Fig. 5. Trace element variation diagrams for the VF lavas. The subscript for the trace element denotes the analytical method where x = XRF and i = ICP-MS. (a) $Zr_x$, (b) $Rb_x$, (c) $Sc_x$, (d) $Nb_i$, (e) $Ba_i$, (f) $La_i$, (g) $Ce_i$, (h) $Pb_i$, (i) $Th_i$, and (j) $U_i$ versus MgO. The light gray-shaded region again outlines the field for the BVF cinder cones (Walker et al., 1995, 2000; Cameron, 1998). Higher degrees of melting for the VF lavas explain the shift to lower incompatible trace element concentrations compared with the field for BVF cinder cones.

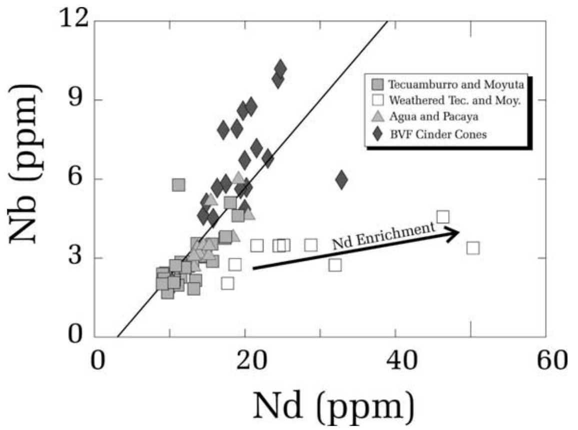


Fig. 6. The Nb versus Nd diagram helps to identify lava samples that have been affected by weathering. Weathered samples plainly diverge from the general trend defined by both VF and BVF magmas. Enrichments in Nd account for this disparate trend.

Baker, 1984), and therefore trajectories will vary from one arc to another. The historic Pacaya lavas have slightly higher CaO contents than the other VF samples and even some primitive island arc lavas. This suggests that plagioclase accumulation occurred in very shallow level magma chambers (Fig. 7, inset). Least-squares mixing models confirm the overall differentiation history of plagioclase fractionation with subordinate pyroxene and olivine crystallization (Cameron, 1998).

The significant differentiation demonstrated for the VF lavas raises legitimate concerns about the degree to which these magmas were contaminated by continental crust. Thick crust and the outcropping of Paleozoic rocks in northwest Guatemala have led to the modification of Sr, Nd, and Pb isotopes by crustal assimilation (Carr et al., 1990; Walker et al., 1995). Four sources have been identified for the Central American arc based on Sr–Nd isotope systematics (Fig. 8a). VF lavas from northwestern Guatemala extend in the direction of local continental crust. Otherwise, Central American stratovolcanoes define an array with a positive slope that represents a mix between a relatively enriched MORB (EM) source and the subducted slab. The slab source itself represents a mix between a depleted MORB (DM) source and sediments plus altered MORB lavas from DSDP Site 495. Behind-the-front volcanism defines the mantle array with cinder cones from Lago Yojoa in Honduras on the depleted end and cinder cones from southeastern Guatemala towards the enriched end. Thus, where thinner and younger crust exists in southeast Guatemala, El Salvador, Nicaragua, and northern Costa Rica (Carr, 1984), the radiogenic isotopic data for the VF lavas show little evidence for crustal assimilation.

The Sr isotopic data we have collected on the Guatemalan VF samples affirm the lack of significant crustal contamination. The VF lavas from southeastern Guatemala show remarkably uniform values of $^{87}Sr/^{86}Sr$ (0.70363–0.70389). A range of reasonable assimilation–fractional crystallization (AFC) models indicates that $^{87}Sr/^{86}Sr$ values would increase sharply towards the field of local continental crust (Fig. 8b). In such AFC models, the relative amount of plagioclase fractionation compared to mafic minerals dictates the value of $D^{Sr}$ (DePaolo, 1981). A BVF cinder cone lava sample (GUC-837) was chosen as the parent material and G1, a granitic sample from southeast Guatemala, was adopted as the assimilant. In all likelihood, $r$ and $D^{Sr}$ change during the course of magma evolution. At depth, the rate of assimilation will approximately equal the rate of crystallization (i.e. $r \cong 1$) and $D^{Sr}$ will be substantially less than 1 owing to the crystallization of mafic phases. As magma ascends to shallow depths in the crust, crystallization thrives at the expense of assimilation leading to a decrease in $r$ (DePaolo, 1981). Plagioclase becomes a more important fractionating phase and $D^{Sr}$ declines. Thus by selecting values of $r$ (e.g. 0.6) and $D^{Sr}$ (0.6–1.0) that portray the advanced stage of differentiation experienced by the VF lavas, the AFC models, although simple, are accurate and geologically applicable. The near-horizontal trend of the VF lavas suggests that either assimilation did not accompany fractional crystallization in a significant manner or, if it did, that the crustal assimilant was not granitic, but a lithology, yet unsampled, more similar to the parent lava in its Sr isotopic composition.

The emphasis placed on diagnostic trace element ratios in upcoming sections justifies close

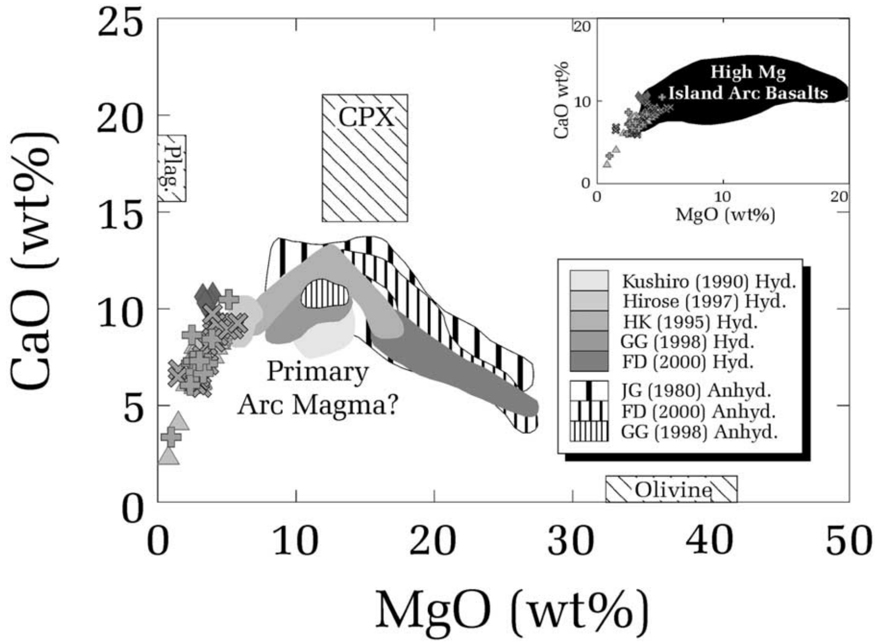


Fig. 7. The CaO versus MgO diagram illustrates the differentiated nature of the VF lavas (after Davidson, 1996). The VF lavas have much lower MgO contents than primary arc magmas. Vertical hatching defines the fields of experimental melts produced by anhydrous peridotite (Jacques and Green, 1980; Gaetani and Grove, 1998; Falloon and Danyushevsky, 2000). Darker shades of gray mark the fields for experimental melts generated from hydrous peridotite (Kushiro, 1990; Hirose and Kawamoto, 1995; Hirose, 1997; Gaetani and Grove, 1998; Falloon and Danyushevsky, 2000). The hydrous experiments more accurately simulate melting conditions in arcs, and therefore, their products better approximate primary arc magmas. In both groups of experiments, MgO contents can range widely with increasing degrees of partial melting. Actual compositions of mineral phases from VF lavas were used to construct the fields for olivine, clinopyroxene, and plagioclase (Cameron, 1998). Inset: the VF lavas only slightly overlap the field of primitive island arc basalts (Kamenetsky et al., 1997; Peate et al., 1997; Hochstaedter et al., 1996a). Experimental melts derived from hydrous peridotite more closely correspond to the high-Mg island arc basalt field.

inspection of the influence differentiation exerts on these critical ratios in VF lavas. We can limit the amount of variability expected in the ratios by incorporating trace elements with similar degrees of high to moderate incompatibility. Consequently, at the source, the probable range of partial melting (e.g. 5–25%) of the mantle wedge beneath Central America would produce very little change in the incompatible trace element ratios. Later at more shallow depths, only minor variations in the ratios would be predicted for subsequent AFC processes. Four of these critical ratios are plotted against MgO in Fig. 9. No clear relationship exists between U/La, Ba/Th, Pb/Ce, and $Th/Rb_N$ and MgO at moderate to high MgO concentrations suggesting that differentiation does not account for the observed trace element ratio variability. Material transfer processes involving the subducted slab are potentially more effective at creating variations in incompatible element ratios in the VF lavas.

### 6.3. The character of slab inputs

In recent years, with the recognition of the mantle wedge as the predominant source, the debate surrounding arc magma genesis has shifted to the nature of slab inputs to the mantle wedge and the exact processes that effect this transfer. The contentious issue now centers on whether fluids or melts from the subducted sediments and/or oceanic crust compose the metasomatic agent. The high recycling efficiency of Be, Nd, Nb, Ta, and Th (i.e. all elements with moderately low fluid

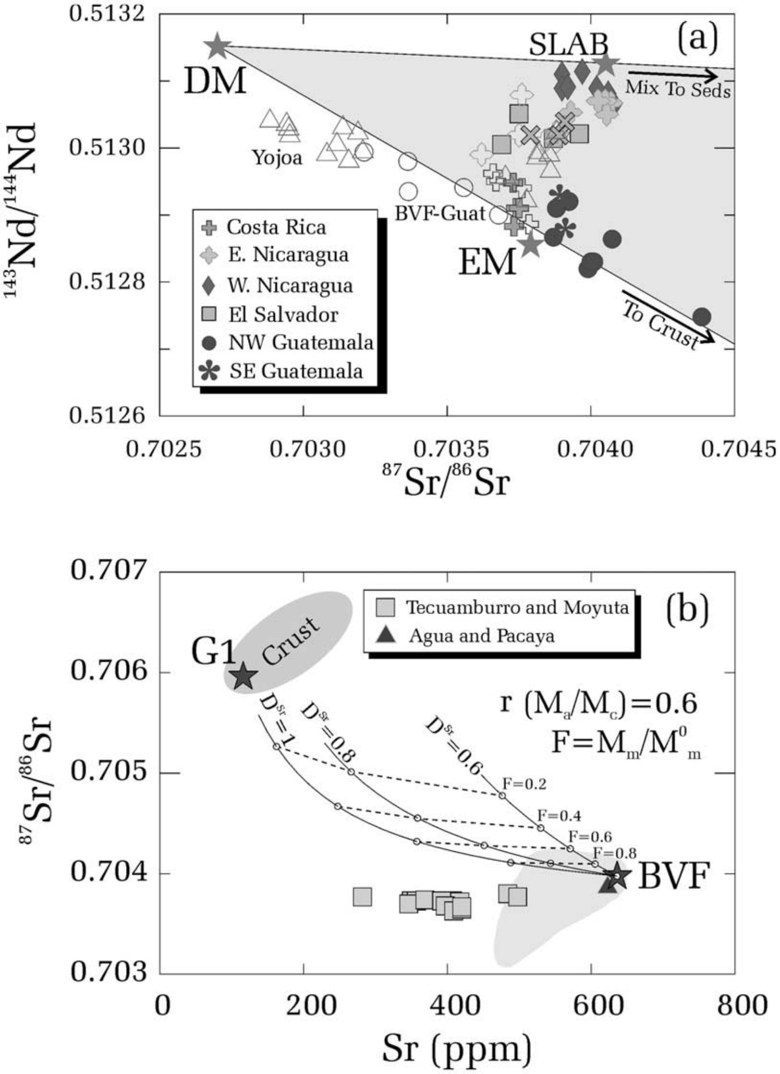


Fig. 8. Assessments of crustal contamination in the entire Central American arc and in southeast Guatemala. (a) The $^{143}Nd/^{144}Nd$ versus $^{87}Sr/^{86}Sr$ diagram shows evidence for crustal contamination in some VF lavas from northwestern Guatemala. Otherwise, VF samples from southeastern Guatemala plot with other Central American lavas on a mixing line between EM and a slab component associated with the subducted sediments. Solid symbols are VF lavas (Carr et al., 1990) and open symbols are back-arc samples. BVF cinder cone samples from Yojoa in Honduras (Patino et al., 1997) and Guatemala (Walker et al., 1995, 2000) define the mantle array. (b) The $^{87}Sr/^{86}Sr$ versus Sr diagram suggests that AFC processes were not significant in the evolution of the VF lavas. The VF lavas do not plot along AFC curves defined by values of $D^{Sr}$ between 0.6 and 1 and $r = 0.6$. The sample from Pacaya plots very close to the chosen parent, a BVF cinder cone sample.

mobility) in some arcs suggests sediment melting is required to explain their transfer to the wedge and eventual incorporation into the volcanic output products (Morris et al., 1990; Cousens et al., 1994; Vroon et al., 1995; Hawkesworth et al., 1997; Hoogewerf et al., 1997; Turner et al., 1997; Shimoda et al., 1998; Johnson and Plank, 1999). Others convincingly argue that the characteristic arc geochemical fingerprint of enrichment in LILEs and depletions in HFSEs supports an

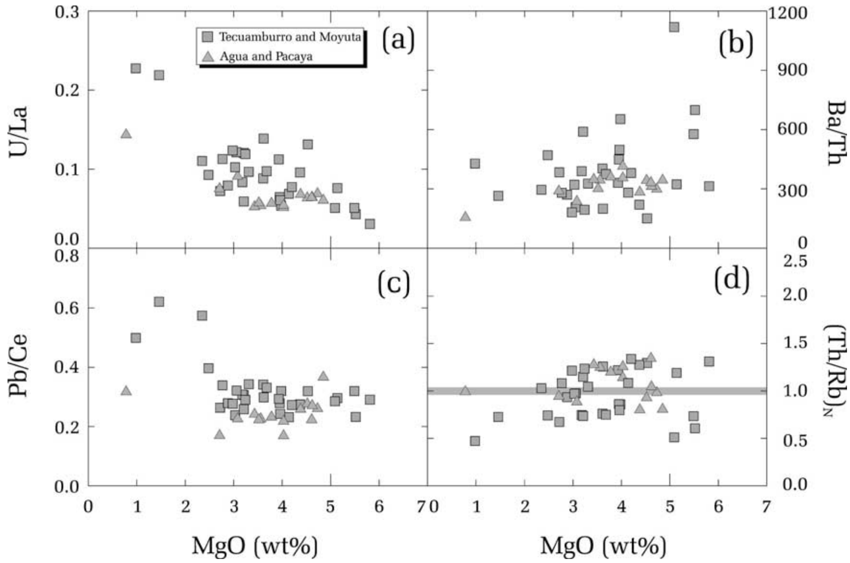


Fig. 9. Variation of critical trace element ratios with differentiation. (a) U/La, (b) Ba/Th, (c) Pb/Ce, and (d) $(Th/Rb)_N$ versus MgO. Except for a slight increase in U/La with increasing differentiation, these key ratios show very little systematic variation with decreasing MgO contents. The lack of systematic variation with MgO suggests that there is no obligation to consider only the most mafic samples.

evolved fluid as the predominant component from the subducted slab (Kersting and Arculus, 1995; Ishikawa and Tera, 1997; Shibata and Nakamura, 1997). The persuasive arguments of both sides have led to the suggestion that a mixed slab flux modifies the mantle wedge in subduction zones (Bau and Knittle, 1993; Ryan et al., 1995; Kepezhinskas et al., 1997; Regelous et al., 1997; Turner and Hawkesworth, 1997; Elliot et al., 1997; Kamenetsky et al., 1997; Peate et al., 1997). Moreover, the contributions from both the subducted sediment and the altered oceanic crust may be separated in time and space (Elliot et al., 1997; Turner and Hawkesworth, 1997; Class et al., 2000). In the Sunda and Tofua arc, hydrous fluids influence melting at the VF, whereas sediment melts may prevail at deeper levels in the rear-arcs (Hoogewerf et al., 1997; Stolz et al., 1996; Kamenetsky et al., 1997). Conversely, a significant sediment component modifies the mantle wedge in the Vanuatu arc except at the rear-arc island of Merelava where signatures of fluid from oceanic crust dominate (Peate et al., 1997).

In the Central American arc, one successful approach to identifying the transfer agent between the subducted slab and the mantle wedge is to compare the mass flux into and out of the subduction zone (Patino et al., 2000). Output/input ratios measure the efficiency of recycling trace elements through the subduction zone and might provide clues to the nature of the subduction component. High output/input ratios (i.e. high recycling efficiency) for fluid-mobile elements such as Cs, B, K, Rb, Sr, U, and Ba reflect the importance of fluid additions to the mantle wedge along the length of the Central American arc (Patino et al., 2000). Furthermore, the relatively poor efficiency in the recycling of Be, Th, and Nb suggests that sediment melts played only a subordinate role in the generation of magma (Patino et al., 2000).

The distinct chemical signature of the hemipelagic and carbonate sediments subducted beneath Central America (Patino et al., 2000) greatly increases the chances for detection in the volcanic output. U/La and Ba/Th distinguish the hemipelagic and carbonate components, respectively (Patino et al., 2000). These ratios share the form of fluid-mobile incompatible element occupying the numerator and fluid-immobile element resid-

Table 3
Compositions of components used in the forward models

| Element | Mature oceanic crust[a] | Hemipelagic sediment[b] | Carbonate sediment[b] | Fluid from oceanic crust[c] | Fluid from hemipelagic sediment[d] | Melt of hemipelagic sediment[e] | Fluid from carbonate sediment[f] | EM source[g] |
|---|---|---|---|---|---|---|---|---|
| U | 0.3 | 4.89 | 0.15 | 5.0 | 246 | 327 | 8.9 | 0.027 |
| La | 1.8 | 9.59 | 3.70 | 4.4 | 50 | 523 | 49 | 0.967 |
| Ba | 23 | 3941 | 2145 | 432 | 358599 | 390237 | 214076 | 8.594 |
| Th | 0.3 | 3.00 | 0.16 | 0.5 | 6.9 | 255 | 9.4 | 0.091 |

[a] From the Geochemical Earth Reference Model (GERM) web site (www-ep.es.llnl.gov/germ/).
[b] Mean hemipelagic and carbonate sediment compositions from Patino et al. (2000).
[c] Calculated assuming 5 wt% fluid flux from an eclogite (cpx:gt = 50:50) and the mineral–aqueous fluid partition coefficients of Brenan et al. (1995) and Stalder et al. (1998) modified slightly for increased mobility of U relative to Th based on calculated uranium and thorium solubilities in subduction zone fluids (Bailey and Ragnarsdottir, 1994).
[d] Calculated assuming 1 wt% fluid flux from a quartz eclogite (cpx:gt:qtz = 45:45:10) and the mineral–aqueous fluid partition coefficients of Brenan et al. (1995) and Stalder et al. (1998) modified slightly as above and with $D_{quartz-fluid} = 0$ for all elements.
[e] Calculated assuming 1 wt% batch melting of a quartz eclogite (cpx:gt:qtz = 45:45:10) and the mineral–melt partition coefficients of Halliday et al. (1995) with $D_{quartz-melt} = 0$ for all elements.
[f] Calculated assuming 1 wt% fluid flux from a limestone (calcite = 100) and assuming $D_{calcite-fluid} = D_{cpx-fluid}$ (Brenan et al., 1995; Stadler et al., 1997).
[g] Calculated by assuming 15% degree melting of EM (Sun and McDonough, 1989).

ing in the denominator. As such, these ratios fit the criteria established by Ryan et al. (1995) and effectively measure a specific subduction component in the Guatemalan lavas.

Forward modeling enables us to generate putative melts and fluids from the sediments and the oceanic crust using published partition coefficients and the modal batch melting equation (Shaw, 1970). Table 3 summarizes the results of such calculations performed in this study. Bearing in mind that the quality of the partition coefficient data limits the resolution of the forward models, we favor this approach to the alternative of bulk sediment contributions. Despite this caveat, the forward models serve a fruitful purpose and provide insight into the possible character of the material transfer agent. In log-plots of U/La versus Ba/Th, arc lavas from Central America showed both local and regional variations (Patino et al., 2000). Regional differences exist in the overall intensity of the slab signature, and local differences occur in the composition of the slab input. Lavas from Nicaragua possess the strongest slab signature, whereas Costa Rica and Guatemala experienced weaker slab inputs. Consequently, Nicaraguan lavas plot farther from the mantle end member than lavas from either Guatemala or Costa Rica (Patino et al., 2000). The local variation spans a compositional spectrum from U/La-rich to more Ba/Th-rich. The hemipelagic sediments show enrichments in both Ba and U, the carbonate sediments have high Ba only, and the oceanic crust is relatively enriched in U over Ba. Interestingly, each segment of the arc, some back-arc regions, and even individual volcanoes exhibit this local variation. The weak slab signature displayed by the expanded data set for VF lavas (Fig. 10a) from southeastern Guatemala supports the along-arc study (Patino et al., 2000). The older stratovolcanoes of Tecuamburro and Moyuta exhibit much more variation (both regional and local) than the younger edifices of Pacaya and Agua even when discounting the weathered samples and highly evolved rocks with less than 2 wt% MgO. The negative array on the U/La versus Ba/Th diagram reflects the local variation in the VF lavas from southeastern Guatemala. Lavas with higher U/La might represent magmas generated from a mantle wedge influenced by fluids (~2%) largely from the oceanic crust. Those lavas with higher Ba/Th were probably produced from partial melting of a source modified by fluids (up to 0.05%) from a carbonate–hemipelagic sediment mix or even just fluids from carbonate sedi-

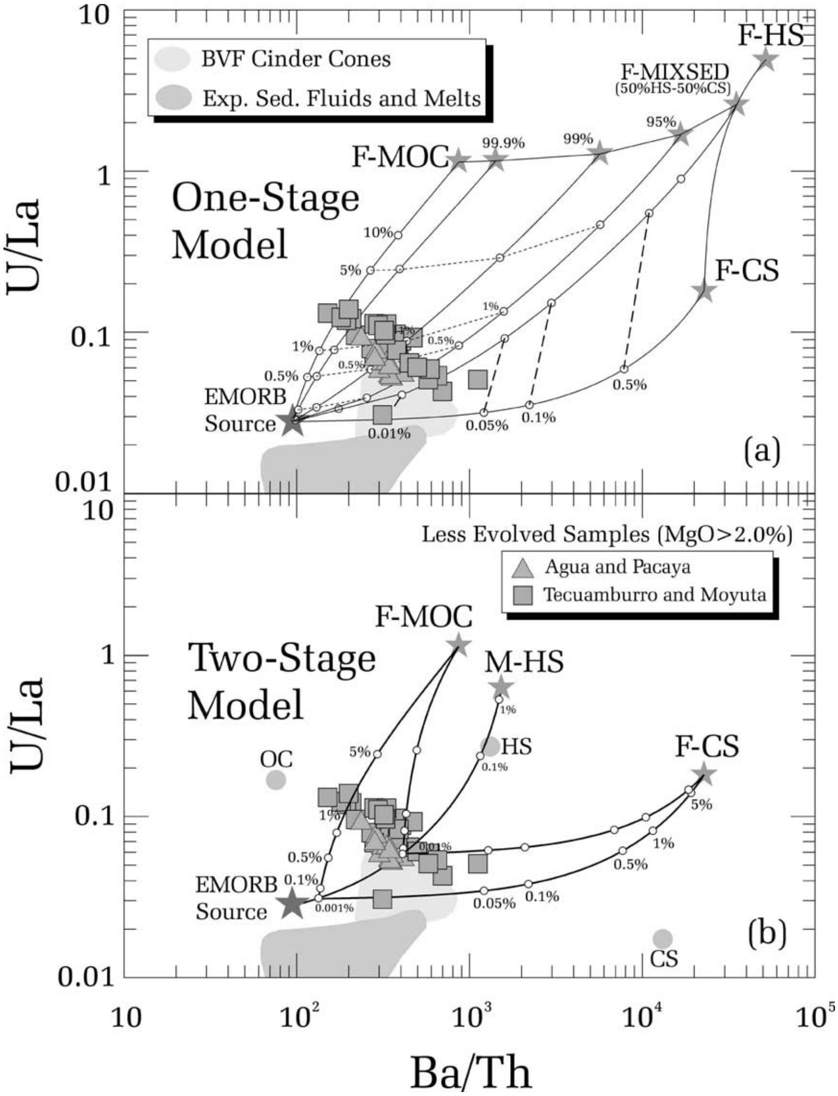


Fig. 10. Geochemical forward models to understand the character of the slab input. Calculated slab components from Table 3 produce distinct mixing curves on the U/La versus Ba/Th diagrams. Tick marks on the mixing curves represent percentages of slab component added to a EM source. Only VF lavas with MgO greater than 2.0 wt% are plotted. Fields for BVF cinder cones (Walker et al., 1995, 2000) and sediment fluids and melts produced by experiments (Johnson and Plank, 1999) are shown for comparison. (a) In a one-stage melting model, fluids derived from the mature oceanic crust (F-MOC), carbonate (F-CS), and hemipelagic sediments (F-HS) induce melting in an EM source to generate the more mafic VF lavas. F-MIXSED is a fluid derived from a sediment mix with equal proportions of the hemipelagic and carbonate components. Fine dashed line shows equivalent contributions from a fluid largely originating from the oceanic crust. Coarse dashed line displays equivalent inputs from a fluid derived from the sediments. (b) In a more realistic two-stage model, melts from the subducted hemipelagic sediments (M-HS) modify the EM source followed by fluid inputs from either mature oceanic crust or carbonate sediments. Bulk slab components are shown as light gray circles where OC = oceanic crust, CS = carbonate sediment, and HS = hemipelagic sediment.

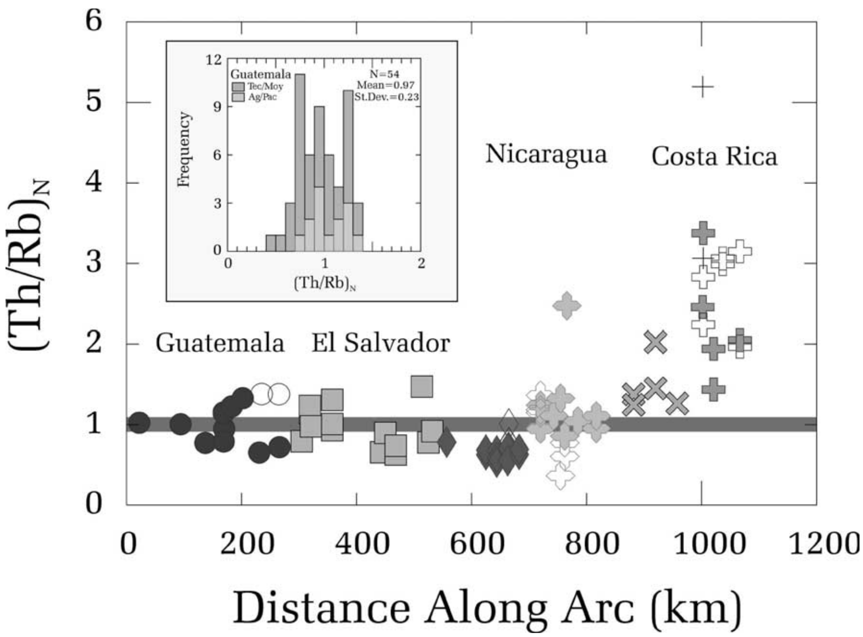


Fig. 11. $(Th/Rb)_N$ is the Th/Rb ratio in the sample normalized to that in the subducting sediment (Johnson and Plank, 1999). The mean Th/Rb in the hemipelagic sediment off Guatemala is 0.074 (Patino et al., 2000). $(Th/Rb)_N$ versus distance along the Central American arc shows that the ratio stays close to 1 for the northern part of the arc. Based on experimental evidence (Johnson and Plank, 1999), a $(Th/Rb)_N$ of $\sim$1 favors sediment melting over sediment dehydration. Solid symbols are VF samples and open symbols are back-arc samples from the Central American arc (Carr et al., 1990). Inset: a histogram of $(Th/Rb)_N$ by ICP-MS in the VF lavas from southeastern Guatemala reveals a mean $(Th/Rb)_N$ ratio of 0.97 with a standard deviation of 0.23.

ment (Fig. 10a). The field for BVF cinder cones occurs at lower U/La ratios suggesting a prominent role for fluids from the subducted sediments in their generation (Fig. 10a).

Although hydrous fluid fluxing of the mantle wedge can explain all the LILE variations in VF lavas, the role of sediment melting requires serious assessment. Recent phase equilibria and trace element partitioning experiments on pelagic red clay have addressed the fate of subducted sediments (Johnson and Plank, 1999). The experiments examine whether critical tracer elements such as Th, Be, and Rb are liberated during sediment dehydration or melting. Arcs with a high Rb flux including Guatemala seem to inherit the sediment ratio meaning that subduction zones recycle Th and Rb equally well. The Th/Rb ratio of hemipelagic sediments off Guatemala is 0.074 (Patino et al., 2000), almost half the value for EM (0.12) or the upper altered oceanic crust (0.13). In the experiments, at the lower temperatures of dehydration $(Th/Rb)_N$, where N signifies normalization to the Th/Rb ratio found in the sediment, is less than 0.5. The $(Th/Rb)_N$ approaches 1.0 only when the solidus is crossed above 750°C. When normalized to the Th/Rb ratio of hemipelagic sediments from DSDP 495, $(Th/Rb)_N$ hovers around 1.0 over the entire Central American arc except for lavas from Costa Rica where the Galapagos plume may cause discrepancies (Fig. 11). VF lavas from southeastern Guatemala have a mean $(Th/Rb)_N$ of 0.97 with a standard deviation of 0.23 based on 54 ICP-MS trace element analyses (Fig. 11, inset). For the subducted sediments to imprint their distinct Th/Rb on the VF lavas requires melting of the sediment.

Thus we present a two-stage fluxing model as a more plausible melting scenario for the VF stratovolcanoes from southeastern Guatemala. Stage 1 would involve the production of a small-degree

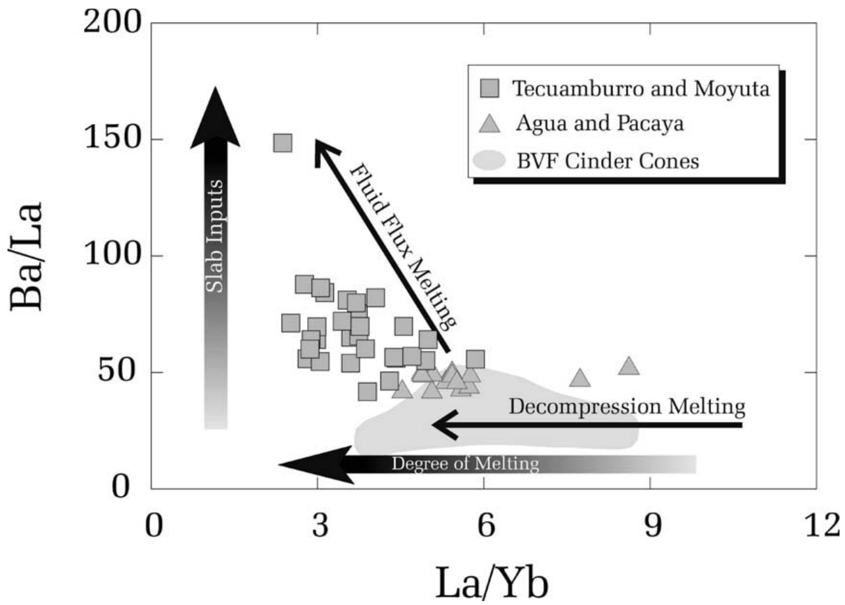


Fig. 12. The Ba/La versus La/Yb diagram serves to identify the main melting process in the mantle wedge. The slab input measured by Ba/La controls the degree of melting recorded by La/Yb in the VF lavas from Tecuamburro and Moyuta. The correlation implies that fluid flux melting generated these magmas. VF lavas from Agua and Pacaya resemble BVF cinder cones and show no relationship between slab additions and extent of melting. Decompression melting was more important in the generation of these VF lavas.

silicic melt from the hemipelagic sediments (Fig. 10b). These sediment melts ($\sim$0.01%) would infiltrate the wedge and create enhanced LILE enrichment in the mantle source. The mantle wedge that spawned the Agua and Pacaya lavas was influenced by slightly smaller percentages of sediment melting. During stage 2, fluid ($\sim$1%) liberated from the oceanic crust would induce melting to create the U/La-enriched magmas and fluid ($\sim$0.05%) from carbonate sediment would instigate melting to generate the Ba/Th-enriched magmas (Fig. 10b). In most cases, this fluid flux interacts with packages of mantle material modified by the sediment melt. This two-stage model involving both sediment melts and fluid fluxes closely agrees with melting scenarios suggested for Nicaragua based on uranium series and $^{10}$Be evidence (Reagan et al., 1994).

Pacaya was singled out for its high organic carbon sediment inputs based on helium and carbon isotopes of its high temperature volcanic gases (Sano and Williams, 1996). Interestingly, the relatively enriched carbon isotopic composition of low-temperature fumaroles at Zunil in the Guatemalan Highlands suggests extremely low organic carbon sediment additions. For two VF stratovolcanoes in Guatemala to have sediment from opposite ends of the organic spectrum implies a crustal carbon source, significant along-arc variations in the subduction component, or some physical process during subduction that generates selective incorporation. Owing to the parallel enrichment of organic carbon (up to 2.4%) and uranium (up to 8 ppm) in the upper 100 m of DSDP Site 495, uranium concentration in the VF lavas might be particularly sensitive to organic sediment inputs to the melt generation zone. The Pacaya and Agua samples straddle the mixing line between an EM source and a hemipelagic sediment melt. Little or no overprinting by a fluid signature is required to explain the Agua–Pacaya mafic samples (Fig. 10b). Thus the organic/hemipelagic sediment signature in the Pacaya lavas revealed by the trace elements provides first order affirmation of the independent volcanic gas study.

### 6.4. Melt generation processes

High equilibrium temperatures at shallow subcrustal levels and nearly $H_2O$-free, high-$CO_2$ mafic glass inclusions in olivines from high-magnesium basalts in western Java strongly suggest that pressure-release melting can take place beneath VF stratovolcanoes (Sisson and Bronto, 1998). In the Cascades, basalts and magnesian basaltic andesites were generated from a heterogeneous mantle source with at least three end members ranging between MORB source, OIB source, and a depleted source strongly enriched in a modern subduction component (Bacon et al., 1997; Borg et al., 1997). Decompression melting was shown to produce the hot, dry high-alumina olivine tholeiites (Bacon et al., 1997; Borg et al., 1997). In the absence of volatile measurements of melt inclusions in olivines, the whole-rock geochemical data on VF stratovolcanoes in Guatemala should help determine the melt generation process in the mantle source. Certainly, the LILE ratios above MORB level lead to the suggestion that slab fluids influenced mantle wedge melting to produce the VF lavas from southeastern Guatemala. Perhaps even more definitive geochemical evidence exists. Flux melting operates as an open system process (Gribble et al., 1996) so that measures of slab input should correlate with the extent of melting (Hochstaedter et al., 1996b). No correlation need exists between the magnitude of slab input and degree of melting for decompression melting, a closed system process. Ba/La, as an estimate of the slab flux, plotted against La/Yb, a suitable gauge for degree of melting of a homogeneous source, investigates the nature of this relationship (Fig. 12). A high degree of LREE mobilization from the slab would reduce the effectiveness of La/Yb as a measure of degree of mantle melting. The steeper negative trend of the lavas from the older stratovolcanoes of Tecuamburro and Moyuta supports flux melting as increases in the slab input raise the extent of melting. In sharp contrast, the lavas from Agua and Pacaya exhibit a horizontal trend that merges with the low Ba/La end of the Tecuamburro–Moyuta data. The absence of any relationship between slab input and degree of melting favors

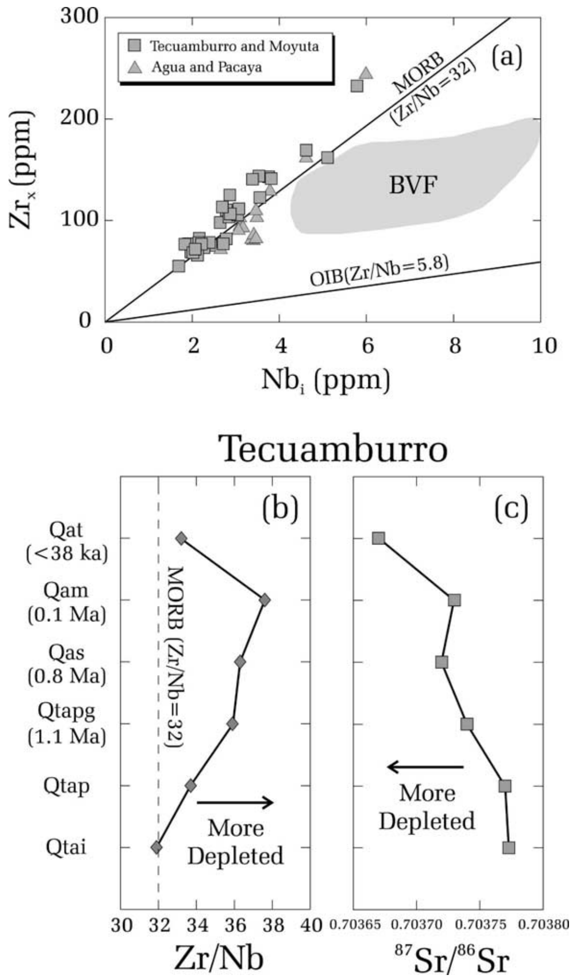


Fig. 13. Insights into the nature and evolution of the mantle wedge. (a) Slab inputs do not change HFSE abundances in the mantle wedge. The high Zr/Nb ratio (>32) of the VF lavas suggests a mantle wedge slightly more depleted than a NMORB source. The VF lavas show little compositional similarity to the BVF cinder cones, which plot on the enriched side of NMORB. NMORB and OIB values from Sun and McDonough (1989). (b) At Tecuamburro volcano, the Zr/Nb ratio has remained higher than the MORB value of 32 over the last 3 Myr. Except for the most recent Tecuamburro lavas, there is a suggestion of source depletion in the Zr/Nb data. (c) Sr isotope ratios of the Tecuamburro lavas suggest that the mantle wedge has become systematically more depleted with time. Abundant BVF volcanism in southeastern Guatemala may account for this depletion trend.

a more prominent role for decompression melting beneath Agua and Pacaya. The Agua and Pacaya data plot close to the field of BVF cinder cones. Walker et al. (1995) suggested decompression melting near the top of the wedge produced the BVF magmas erupted at the cinder cones. The rate of extension rather than the slab flux would exert more control on the extent of decompression melting. Pacaya's location on the actively deforming Chortis microblock at the junction of the dextral Jalpatagua fault and the Guatemala City graben results in active extension (Conway, personal communication, 1997). Relatively rapid ascent in an extensional setting contributes to the narrow composition range for modern lavas at Pacaya.

### 6.5. Nature of the mantle source

Debate continues over the chemical nature of the mantle wedge that serves as the primary source for arc magmas. Disagreement centers on whether the mantle wedge chemically resembles an enriched OIB source (Reagan and Gill, 1989; Morris and Hart, 1983) or a more DM source (Woodhead et al., 1993; Pearce and Parkinson, 1993). Just as recent partition experiments identify the LILE and the LREE as fluid-mobile trace elements, they also recognize the largely immobile nature of the HFSE and HREE (Keppler, 1996; Brenan et al., 1995; Kogiso et al., 1997). Therefore, variable slab inputs do not affect the primary distributions of HFSE and HREE produced by partial melting of the mantle wedge. The Zr/Nb ratio has remained essentially constant in the VF lavas despite their evolved nature and the effects of incipient weathering (Fig. 13a). The elevated Zr/Nb ratio of the VF lavas indicates that the mantle wedge was slightly more depleted than a MORB source with respect to trace elements (Fig. 13a).

Woodhead et al. (1993) proposed that the depleted material resulting from melt extraction during back-arc magmatism advects into the wedge where fluxes from the slab generate arc magmatism. REE patterns of VF lavas from the Kamchatkan arc provide strong support for this model. Arc rocks with depleted REE patterns occur at the VF front where behind-the-front volcanism thrives, whereas relatively enriched REE patterns characterize those portions of the front where BVF magmatism was missing (Hochstaedter et al., 1996a). Simple tests of the depletion model include a comparison of wedge fertility at arcs with and without back-arc systems, and an examination of wedge fertility through time in subduction zones with both arc and back-arc systems. With respect to the first test, this study confirms that VFs with accompanying back-arc magmatism have trace element ratios that indicate depleted sources.

Age dating at Tecuamburro volcano (Duffield et al., 1992) also makes it possible to undertake the latter test by monitoring changes in the chemical nature of the mantle wedge through time. Detailed mapping and geochronologic studies suggest that major stratovolcanoes in arc settings remain active for 500 kyr to $\sim 1$ Myr (Hildreth and Lanphere, 1994; Singer et al., 1997). During this extended period, changes may occur in vent position, magma composition, and eruptive processes. In terms of Zr/Nb ratio, lavas become progressively more depleted except for a recent enrichment period recorded in Tecuamburro lavas younger than around 0.1 Ma (Fig. 13b). Modern Pacaya lavas have a mean Zr/Nb ratio of 24.6 and seem to also register a relatively enriched mantle signature. The $^{87}Sr/^{86}Sr$ ratios of the Tecuamburro lavas show more systematic behavior. It is worth noting that the Tecuamburro lavas are more enriched in $^{87}Sr/^{86}Sr$ than even EM. However, the Sr isotopic values of the Tecuamburro rocks do become more depleted with time. The mean $^{87}Sr/^{86}Sr$ ratio declines from 0.703773 in the oldest rocks of the Ixhautan complex (Qtai) to 0.703670 in the youngest unit (Qat). The older lava flows were erupted prior to the onset of BVF volcanism in southeastern Guatemala. The younger lava flows from Tecuamburro volcano were erupted coevally, or possibly even subsequent to BVF cinder cone volcanism. The restriction of isotopically more depleted arc lavas to the syn- or post-cinder cone period of activity at Tecuamburro volcano provides some preliminary support to the depletion model outlined above.

## 7. Summation and conclusions

VF lavas from adjacent segments in the Central American arc exhibit the characteristic arc geochemical fingerprint of enrichments in LILE and depletions in HFSE on trace element primitive mantle-normalized diagrams. The high Ba/Th ratios of the VF lavas classified them as forming in a depleted arc according to the scheme of Hawkesworth et al. (1997). Fractional crystallization of plagioclase, clinopyroxene, and subordinate olivine has modified primary magma compositions, but did not lead to recognizable crustal contamination. Extensive assimilation in Central America has been restricted to northwestern Guatemala where crustal thickness exceeds 45 km. Critical trace element ratios remain largely unchanged during the differentiation process. The large-scale mobility of the REE caused by incipient weathering warranted concern especially at Tecuamburro and Moyuta. Samples of older lavas modified by weathering were identified based on relative enrichments in the REE and omitted from consideration in the petrogenetic discussion.

At the present time, forward modeling offers only a qualitative assessment of the slab contributions to the mantle. In a regional context, the detailed geochemical data reported in this study confirmed the diminutive slab flux registered by the VF lavas. Tecuamburro and Moyuta samples exhibit much more variability than Agua and Pacaya with respect to key trace element ratios involving LILE. This variability defines a local trend that depends more on the proportion and nature of the slab input. As in other arcs (e.g. Elliot et al., 1997), bulk mixing of sediments with the mantle wedge cannot explain the local trend because many lavas plot outside the bulk mixing curves (see Patino et al., 2000). Mixing curves between EM and putative fluids and melts from the subducted slab better constrain the Guatemalan data. A simple one-stage model suggests that the VF lavas can be derived from a mantle metasomatized by fluids from various combinations of oceanic crust, hemipelagic sediment, and carbonate sediment. Steep angles of subduction might induce deeper fractures in the slab to account for the high fluid fluxes from the oceanic crust (Kirby, 1995; Patino et al., 2000). Based on recent dehydration and melting experiments on pelagic red clay (Johnson and Plank, 1999), $(Th/Rb)_N$ ratios of $\sim 1$ in the VF lavas from southeastern Guatemala imply sediment melting. In a two-stage model, the VF basalts can be generated by first mixing the mantle with small-degree melts from the hemipelagic sediments and then adding a fluid component either from the oceanic crust or the carbonate sediment.

Low volatile contents in melt inclusions hosted by olivines from VF lavas demonstrate that decompression melting occurs in arc settings (Sisson and Bronto, 1998). The fact that Ba/La, a measure of overall slab input, correlates well with La/Yb, a measure of the extent of melting, for lavas from Tecuamburro and Moyuta supports the open system flux melting process. In sharp contrast, the lack of correlation between measures of slab input and degree of melting for lavas from Agua and Pacaya suggests that decompression melting was more important. Pacaya lies in an extensional regime at the intersection between the Jalpataugua fault and the Guatemala City graben. In this setting, the rate of extension controlled the degree of melting and also facilitated magma to ascend rapidly to the surface inhibiting extensive differentiation in the recent lavas.

Tecuamburro volcano offers the best chance to capture changes in the chemical character of the mantle source because of its protracted activity and the existence of age dates on its main volcanic units (Duffield et al., 1992). In terms of trace elements, the Zr/Nb ratio of the Tecuamburro lavas shows that the mantle wedge was slightly more depleted than MORB. Except for an enrichment trend in the last 100 000 yr, the mantle wedge became progressively more depleted. The Sr isotopic composition of the same units indicates that the mantle wedge has become continuously more depleted in radiogenic Sr with time. These data generally support the hypothesis that back-arc volcanism plays a key role in the depletion of mantle sources in arc environments.

## Acknowledgements

Field work in Guatemala would not have been possible or as enjoyable without the expert assistance of Rodolfo Morales and Sharon Templeton. We gratefully recognize the assistance of Neil

Dickey with the XRF analyses, and the generosity of Clive Neal for access to the ICP-MS laboratory at the University of Notre Dame. Constructive reviews by Charles Bacon and Ian Smith significantly improved the manuscript. The research was supported in part by student grants to B.I.C. from Sigma Xi, the Geological Society of America, and the Center for Latino and Latin American Studies at Northern Illinois University. B.I.C. also thanks the Graduate School at Northern Illinois University for a dissertation completion fellowship. This research was partially supported by Grants from the National Science Foundation to M.J.C. and M.D.F. (NSF EAR 9406624 and NSF EAR 9628251).

## References

Bacon, C.R., Bruggman, P.E., Christiansen, R.L., Clynne, M.A., Donnelly-Nolan, J.M., Hildreth, W., 1997. Primitive magmas at five Cascade volcanic fields: Melts from hot, heterogeneous sub-arc mantle. Can. Mineral. 35, 397–423.

Bailey, E.H., Ragnarsdottir, K.V., 1994. Uranium and thorium solubilities in subduction zone fluids. Earth Planet. Sci. Lett. 124, 119–129.

Bardintzeff, J.-M., Deniel, C., 1992. Magmatic evolution of Pacaya and Cerro Chiquito volcanological complex, Guatemala. Bull. Volcanol. 54, 267–283.

Bau, M., Knittle, U., 1993. Significance of slab-derived partial melts and aqueous fluids for the genesis of tholeiitic and calc-alkaline island-arc basalts: Evidence from Mt. Arayat, Philippines. Chem. Geol. 105, 233–251.

Berg, J.H., Weis, D., Cameron, B.I., 1995. Enriched HIMU source for the Balleny Islands basalts, Southern Ocean. EOS Trans. Am. Geophys. Union 76, F693.

Borg, L.E., Clynne, M.A., Bullen, T.D., 1997. The variable role of slab-derived fluids in the generation of a suite of primitive calc-alkaline lavas from the southernmost Cascades, California. Can. Mineral. 35, 425–452.

Bourdon, B., Turner, S., AllÀgre, C., 1999. Melting dynamics beneath the Tonga-Kermadec island arc inferred from $^{231}Pa$–$^{235}U$ systematics. Science 286, 2491–2493.

Brenan, J.M., Shaw, H.F., Ryerson, F.J., Phinney, D.L., 1995. Mineral–aqueous fluid partitioning of trace elements at 900°C and 2.0 Gpa: constraints on the trace element chemistry of mantle and deep crustal fluids. Geochim. Cosmochim. Acta 59, 3332–3350.

Burkhart, B., Self, S., 1985. Extension and rotation of crustal blocks in northern Central America and effect on the volcanic arc. Geology 13, 22–26.

Cameron, B.I., 1998. Melt Generation and Magma Evolution in Southeastern Guatemala. Unpublished Ph.D. Thesis, Northern Illinois University, DeKalb, IL, 399 pp.

Carr, M.J., 1984. Symmetrical and segmented variation of physical and geochemical characteristics of the Central American volcanic front. J. Volcanol. Geotherm. Res. 20, 231–252.

Carr, M.J., Stoiber, R.E., 1990. Volcanism. In: Dengo, G., Case, J.E. (Eds.), The Caribbean Region. The Geology of North America, Vol. H, pp. 375–391.

Carr, M.J., Feigenson, M.D., Bennett, E.A., 1990. Incompatible element and isotopic evidence for tectonic control of source mixing and melt extraction along the Central American arc. Contrib. Mineral. Petrol. 105, 369–380.

Class, C., Miller, D.M., Goldstein, S.L., Langmuir, C.H., 2000. Distinguishing melt and fluid subduction components in Umnak volcanics, Aleutian Arc. Geochem. Geophys. Geosyst., Vol. 1, Paper number 1999GC000010.

Cousens, B.L., Allan, J.F., Gorton, M.P., 1994. Subduction-modified pelagic sediments as the enriched component in back-arc basalts from the Japan Sea: Ocean Drilling Program Sites 797 and 794. Contrib. Miner. Petrol. 117, 421–434.

Davidson, J.P., 1996. Deciphering mantle and crustal signatures in subduction zone magmatism. In: Bebout, G.E., Scholl, D., Kirby, S., Platt, J.P. (Eds.), Subduction Top to Bottom. Am. Geophys. Union Geophys. Monogr. 96, 251–262.

Davies, J.H., Stevenson, D.J., 1992. Physical model of source region of subduction zone volcanics. J. Geophys. Res. 97, 2037–2070.

Demets, C., Gordon, R.G., Argus, D.F., Stein, S., 1990. Current plate motions. Geophys. J. Int. 101, 425–478.

DePaolo, D.J., 1981. Trace element and isotopic effects of combined wallrock assimilation and fractional crystallization. Earth Planet. Sci. Lett. 53, 189–202.

Duffield, W.A., Heiken, G.H., Wohletz, K.H., Maassen, L.W., Dengo, G., Pinzon, O., 1991. Geologic map of Tecuamburro volcano and surrounding area, Guatemala. Miscellaneous Investigation Series, US Geological Survey, Map I-2197.

Duffield, W.A., Heiken, G.H., Wohletz, K.H., Maassen, L.W., Dengo, G., McKee, E.H., Casteneda, O., 1992. Geology and geothermal potential of the Tecuamburro volcano area, Guatemala. Geothermics 21, 425–446.

Eastell, J., Willis, J.P., 1990. A low dilution fusion technique for the analysis of geological samples. X-Ray Spectrom. 19, 3–14.

Elliot, T., Plank, T., Zindler, A., White, W., Bourdon, B., 1997. Element transport from slab to volcanic front at the Mariana arc. J. Geophys. Res. 102, 14991–15019.

Ewart, A.E., Hawkesworth, C.J., 1987. The Pleistocene–Recent Tonga-Kermadec arc lavas: interpretation of new isotopic and rare-earth data in terms of a depleted source model. J. Petrol. 28, 495–530.

Falloon, T.J., Danyushevsky, L.V., 2000. Melting of refractory mantle at 1.5, 2 and 2.5 GPa under anhydrous and $H_2O$-undersaturated conditions: Implications for the petrogenesis of high-Ca boninites and the influence of subduction components on mantle melting. J. Petrol. 41, 257–283.

Francalanci, L., Taylor, S.R., McCulloch, M.T., Woodhead, J.D., 1993. Geochemical and isotopic variations in the calc-alkaline rocks of Aeolian arc, southern Tyrrhenian Sea, Italy: constraints on magma genesis. Contrib. Mineral. Petrol. 113, 300–313.

Gaetani, G.A., Grove, T.L., 1998. The influence of water on melting of mantle peridotite. Contrib. Mineral. Petrol. 131, 323–346.

Gerbe, M.-C., Gourgaud, A., Sigmarsson, O., Harmon, R.S., Joron, J.-L., Provost, A., 1992. Mineralogical and geochemical evolution of the 1982–1983 Galunggung eruption (Indonesia). Bull. Volcanol. 54, 284–298.

Gertisser, R., Keller, J., 2000. From basalt to dacite: origin and evolution of the calc-alkaline series of Salina, Aeolian Arc, Italy. Contrib. Mineral. Petrol. 139, 607–626.

Gill, J.B., 1981. Orogenic Andesites and Plate Tectonics. Springer, New York, 390 pp.

Goff, F., Janik, C., Fahlquist, L., Adams, A., Roldan, A., Revolorio, M., Trujillo, P.E., Counce, D., 1991. A re-evaluation of the Moyuta geothermal system, southern Guatemala. Geotherm. Resourc. Counc. Trans. 15, 3–10.

Gribble, R.F., Stern, R.J., Bloomer, S.H., Stuben, D., O'Hearn, T., Newman, S., 1996. MORB mantle and subduction components interact to generate basalts in the southern Mariana Trough back-arc basin. Geochim. Cosmochim. Acta 60, 2153–2166.

Grove, T.L., Baker, M.B., 1984. Phase equilibrium controls on the tholeiitic versus calc-alkaline differentiation trends. J. Geophys. Res. 89, 3253–3274.

Halliday, A.N., Lee, D.-C., Tommasini, S., Davies, G.R., Paslick, C.R., Fitton, J.G., James, D.E., 1995. Incompatible trace elements in OIB and MORB and source enrichment in the suboceanic mantle. Earth Planet. Sci. Lett. 133, 379–395.

Hawkesworth, C., Turner, S., Peate, D., van Calsteren, P., 1997. U–Th isotopes in arc magmas: Implications for element transfer from the subducted crust. Science 276, 551–555.

Hildreth, W., Lanphere, M.A., 1994. Potassium-argon geochronology of a basalt-andesite-dacite arc system: The Mount Adams volcanic field, Cascade Range of southern Washington. Geol. Soc. Am. Bull. 106, 1413–1429.

Hirose, K., 1997. Melting experiments on lherzolite KLB-1 under hydrous conditions and generation of high-magnesian andesitic melts. Geology 25, 42–44.

Hirose, K., Kawamoto, T., 1995. Hydrous partial melting of lherzolite at 1 Gpa: The effect of $H_2O$ on the genesis of basaltic magmas. Earth Planet. Sci. Lett. 133, 463–473.

Hochstaedter, A.G., Kepeshinskas, P., Defant, M., Drummond, M., Koloskov, A., 1996a. Insights into the volcanic arc mantle wedge from magnesian lavas from the Kamchatka arc. J. Geophys. Res. 101, 697–712.

Hochstaedter, A.G., Ryan, J.G., Luhr, J.F., Hasenaka, T., 1996b. On B/Be ratios in the Mexican Volcanic Belt. Geochim. Cosmochim. Acta 60, 613–628.

Hoogewerf, J.A., van Bergen, M.J., Vroon, P.Z., Hertogen, J., Wordel, R., Sneyers, A., Nasution, A., Varekamp, J.C., Moens, H.L.E., Mouchel, D., 1997. U-series, Sr–Nd–Pb isotope and trace element systematics across an active island arc-continent collision zone: Implications for element transfer at the slab-wedge interface. Geochim. Cosmochim. Acta 61, 1057–1072.

Hopf, S., 1993. Behavior of rare earth elements in geothermal systems of New Zealand. J. Geochem. Explor. 47, 333–357.

Ishikawa, T., Tera, F., 1997. Source, composition and distribution of the fluid in the Kurile mantle wedge: Constraints from across-arc variations of B/Nb and B isotopes. Earth Planet. Sci. Lett. 152, 123–138.

Iwamori, H., 1998. Transportation of $H_2O$ and melting in subduction zones. Earth Planet. Sci. Lett. 160, 65–80.

Jacques, A.L., Green, D.H., 1980. Anhydrous melting of peridotite at 0–15 Kb pressure and the genesis of tholeiitic basalts. Contrib. Mineral. Petrol. 73, 287–310.

Jenner, G.A., Longerich, H.P., Jackson, S.E., Fryer, B.J., 1990. ICP-MS – a powerful tool for high-precision trace element analysis in Earth Sciences: evidence from analysis of selected USGS reference samples. Chem. Geol. 139, 39–49.

Johnson, M.C., Plank, T., 1999. Dehydration and melting experiments constrain the fate of subducted sediments. Geochem. Geophys. Geosyst., Vol. 1, Paper number 1999GC000014.

Kamenetsky, V.S., Crawford, A.J., Eggins, S., Muhe, R., 1997. Phenocryst and melt inclusion chemistry of near-axis seamounts, Valu Fa Ridge, Lau Basin: Insight into mantle wedge melting and the addition of subduction components. Earth Planet. Sci. Lett. 151, 205–223.

Keleman, P.B., Shimizu, N., Dunn, T., 1993. Relative depletion of niobium in some arc magmas and the continental crust: partitioning of K, Nb, La and Ce during melt/rock reaction in the upper mantle. Earth Planet. Sci. Lett. 120, 111–134.

Kepezhinskas, P., McDermott, F., Defant, M.J., Hochstaedter, A., Drummond, M.S., Hawkesworth, C.J., Koloskov, A., Maury, R.C., Bellon, H., 1997. Trace element and Sr–Nd–Pb isotopic constraints on a three-component model of Kamchatka arc petrogenesis. Geochim. Cosmochim. Acta 61, 577–600.

Keppler, H., 1996. Constraints from partitioning experiments on the composition of subduction-zone fluids. Nature 380, 237–240.

Kersting, A.B., Arculus, R.J., 1995. Pb isotope composition of Klyuchevskoy volcano, Kamchatka and North Pacific sediments: Implications for magma genesis and crustal recycling in the Kamchatkan arc. Earth Planet. Sci. Lett. 136, 133–148.

Kirby, S., 1995. Interslab earthquakes and phase changes in subducting lithosphere. Rev. Geophys. 33 (Suppl.), 287–297.

Kogiso, T., Tatsumi, Y., Nakano, S., 1997. Trace element transport during dehydration processes in the subducted oceanic crust: 1. Experiments and implications for the origin of ocean island basalts. Earth Planet. Sci. Lett. 148, 193–205.

Kuschel, E., Smith, I.A., 1992. Rare earth element mobility in young arc-type volcanic rocks from northern New Zealand. Geochim. Cosmochim. Acta 56, 3951–3955.

Kushiro, I., 1990. Partial melting of mantle wedge and evolution of island arc crust. J. Geophys. Res. 95, 15929–15939.

Langmuir, C.H., Klein, E.M., Plank, T., 1992. Petrological systematics of mid-ocean ridge basalts: Constraints on melt generation beneath ocean ridges. In: Phipps Morgan, J., Blackman, D.K., Sinton, J.M. (Eds.), Mantle Flow and Melt Generation at Mid Ocean Ridges. Geophys. Monogr. Am. Geophys. Union, Washington, DC, 71, 183–280.

LeBas, M.J., LeMaitre, R.W., Streckeisen, A., Zanettin, B., 1986. A chemical classification of volcanic rocks based on the total alkali silica diagram. J. Petrol. 27, 745–750.

Leroy, J.L., Turpin, L., 1988. REE, Th and U behavior during hydrothermal and supergene processes in a granitic environment. Chem. Geol. 68, 239–251.

Lewis, A.J., Palmer, M.R., Sturchio, N.C., Kemp, A.J., 1997. The rare earth element geochemistry of acid-sulphate and acid-sulphate-chloride geothermal systems from Yellowstone National Park, Wyoming, USA. Geochim. Cosmochim. Acta 61, 695–705.

Marsh, J.S., 1991. REE fractionation and Ce anomalies in weathered Karoo dolerite. Chem. Geol. 90, 189–194.

McKenzie, D., O'Nions, R.K., 1998. Melt production beneath oceanic islands. Phys. Earth Planet. Int. 107, 143–182.

Miyashiro, A., 1974. Volcanic rock series in island arcs and active continental margins. Am. J. Sci. 274, 321–355.

Morris, J.D., Hart, S.R., 1983. Isotopic and incompatible element constraints on the genesis of island arc volcanics from Cold Bay and Amak Island, Aleutians, and implications for mantle structure. Geochim. Cosmochim. Acta 47, 2015–2030.

Morris, J.D., Leeman, W.P., Tera, F., 1990. The subducted component in island arc lavas: constraints from Be isotopes and B/Be systematics. Nature 344, 31–36.

Patino, L.C., Carr, M.J., Feigenson, M.D., 1997. Cross-arc geochemical variations in volcanic fields in Honduras C.A.: progressive changes in source with distance from the volcanic front. Contrib. Mineral. Petrol. 129, 341–351.

Patino, L.C., Carr, M.J., Feigenson, M.D., 2000. Local and regional variations in Central American arc lavas controlled by variations in subducted sediment input. Contrib. Mineral. Petrol. 138, 265–283.

Pearce, J.A., Parkinson, I.J., 1993. Trace element models for mantle melting: application to volcanic arc petrogenesis. In: Pritchard, H.M., Alabaster, T., Harris, N.B.W., Neary, C.R. (Eds.), Magmatic Processes and Plate Tectonics. Spec. Publ. Geol. Soc. London 76, 373–403.

Peate, D.W., Pearce, J.A., Hawkesworth, C.J., Colley, H., Edwards, C.M.H., Hirose, K., 1997. Geochemical variations in Vanuatu arc lavas: the role of subducted material and a variable mantle wedge composition. J. Petrol. 38, 1331–1358.

Price, R.C., Gray, C.M., Wilson, R.E., Frey, F.A., Taylor, S.R., 1991. The effects of weathering on rare-earth element, Y, and Ba abundances in Tertiary basalts from southeastern Australia. Chem. Geol. 93, 245–265.

Protti, M., Guendel, F., McNally, K., 1995. Correlation between the age of the subducting Cocos plate and the geometry of the Wadati-Benioff zone under Nicaragua and Costa Rica. In: Mann, P. (Ed.), Geologic and Tectonic Development of the Caribbean Plate Boundary in Southern Central America. Geol. Soc. Am. Spec. Pap. 295, 309–326.

Reagan, M.K., Gill, J.B., 1989. Coexisting calcalkaline and high-niobium basalts from Turrialba volcano, Costa Rica: implications for residual titanates in arc magma sources. J. Geophys. Res. 94, 4619–4633.

Reagan, M.K., Morris, J.D., Herrstrom, E.A., Murrell, M.T., 1994. Uranium series and beryllium isotope evidence for an extended history of subduction modification of the mantle below Nicaragua. Geochim. Cosmochim. Acta 58, 4199–4212.

Regelous, M., Collerson, K.D., Ewart, A., Wendt, J.I., 1997. Trace element transport rates in subduction zones: evidence from Th, Sr, and Pb isotope data for Tonga-Kermadec arc lavas. Earth Planet. Sci. Lett. 150, 291–302.

Regelous, M., Niu, Y., Wendt, J.I., Batiza, R., Greig, A., Collerson, K.D., 1999. Variations in the geochemistry of magmatism on the East Pacific Rise at 10°30′N since 800 ka. Earth Planet. Sci. Lett. 168, 45–63.

Reynolds, J.H., 1987. Timing and sources of Neogene and Quaternary volcanism in south-central Guatemala. J. Volcanol. Geotherm. Res. 33, 9–22.

Roggensack, K., Hervig, R.L., McKnight, S.B., Williams, S.N., 1997. Explosive basaltic volcanism from Cerro Negro volcano: influence of volatiles on eruptive style. Science 277, 1639–1642.

Ryan, J.G., Morris, J., Tera, F., Leeman, W.P., Tsvetkov, A., 1995. Cross-arc geochemical variations in the Kurile arc as a function of slab depth. Science 270, 625–627.

Ryerson, F.J., Watson, E.B., 1987. Rutile saturation in magmas: implications for Ti–Nb–Ta depletion in island arc basalts. Earth Planet. Sci. Lett. 86, 225–239.

Sano, Y., Williams, S.N., 1996. Fluxes of mantle and subducted carbon along convergent plate boundaries. Geophys. Res. Lett. 23, 2749–2752.

Shaw, D.M., 1970. Trace element fractionation during anatexis. Geochim. Cosmochim. Acta 34, 237–243.

Shibata, T., Nakamura, E., 1997. Across-arc variations of isotope and trace element compositions from Quaternary basaltic volcanic rocks in northeastern Japan: Implications for interaction between subducted oceanic crust and mantle wedge. J. Geophys. Res. 102, 8051–8064.

Shimoda, G., Tatsumi, Y., Nohda, S., Ishizaka, K., Jahn, B.M., 1998. Setouchi high-Mg andesites revisited: geochemical evidence for melting of subducted sediments. Earth Planet. Sci. Lett. 160, 479–492.

Singer, B.S., Thompson, R.A., Dungan, M.A., Feeley, T.C., Nelson, S.T., Pickens, J.C., Brown, L.L., Wulff, A.W., Davidson, J.P., Metzger, J., 1997. Volcanism and erosion during the past 930 k.y. at the Tatara-San Pedro complex, Chilean Andes. Geol. Soc. Am. Bull. 109, 127–142.

Sisson, T.W., Bronto, S., 1998. Evidence of pressure-release melting beneath magmatic arcs from basalt at Galunggung, Indonesia. Nature 391, 883–886.

Sisson, T.W., Layne, G.D., 1993. $H_2O$ in basalt and basaltic andesite glass inclusions from four subduction-related volcanoes. Earth Planet. Sci. Lett. 117, 619–635.

Sobolev, A.V., Chaussidon, M., 1996. $H_2O$ concentrations in primary melts from supra-subduction zones and mid-ocean ridges: Implications for $H_2O$ storage and recycling in the mantle. Earth Planet. Sci. Lett. 137, 45–55.

Stalder, R., Foley, S.F., Brey, G.P., Horn, I., 1998. Mineral–aqueous fluid partitioning of trace elements at 900–1200°C and 3.0–5.7 GPa: new experimental data for garnet, clinopyroxene, and rutile, and implications for mantle metasomatism. Geochim. Cosmochim. Acta 62, 1781–1801.

Stolz, A.J., Jochum, K.P., Spettel, B., Hofmann, A.W., 1996. Fluid and melt-related enrichment in the subarc mantle: evidence from Nb/Ta variations in island-arc basalts. Geology 24, 587–590.

Sun, S.S., McDonough, W.F., 1989. Chemical and isotopic systematics of oceanic basalts: Implications for mantle composition and processes. In: Saunders, A.D., Norry, M.J. (Eds.), Magmatism in the Ocean Basins. Geol. Soc. Spec. Publ. 42, 313–345.

Terakado, Y., Fujitani, T., Takada, J., 1993. Experimental study on the sorption of rare-earth elements and other trace elements during rhyolite-hydrothermal water interactions. Chem. Geol. 106, 317–330.

Turner, S., Hawkesworth, C., 1997. Constraints on flux rates and mantle dynamics beneath island arcs from Tonga-Kermadec lava geochemistry. Nature 389, 568–573.

Turner, S., Hawkesworth, C., van Calsteren, P., Heath, E., Macdonald, R., Black, S., 1996. U-series isotopes and destructive plate margin magma genesis in the Lesser Antilles. Earth Planet. Sci. Lett. 142, 191–207.

Turner, S., Hawkesworth, C., Rogers, N., Bartlett, J., Worthington, T., Hergt, J., Pearce, J., Smith, I., 1997. $^{238}U/^{230}Th$ disequilibria, magma petrogenesis, and flux rates beneath the depleted Tonga-Kermadec island arc. Geochim. Cosmochim. Acta 61, 4855–4884.

Turner, S., McDermott, F., Hawkesworth, C., Kepezhinskas, P., 1998. A U-series study of lavas from Kamchatka and the Aleutians: constraints on source composition and melting processes. Contrib. Mineral. Petrol. 133, 217–234.

Vroon, P.Z., van Bergen, M.J., Klaver, G.J., White, W.M., 1995. Strontium, neodymium, and lead isotopic and trace-element signatures of the East Indonesian sediments: Provenance and implications for Banda arc magma genesis. Geochim. Cosmochim. Acta 59, 2573–2598.

Walker, J.A., Carr, M.J., Patino, L.C., Johnson, C.M., Feigenson, M.D., Ward, R.L., 1995. Abrupt change in magma generation processes across the Central American arc in southeastern Guatemala: flux-dominated melting near the base of the wedge to decompression melting near the top of the wedge. Contrib. Miner. Petrol. 120, 378–390.

Walker, J.A., Patino, L.C., Cameron, B.I., Carr, M.J., 2000. Petrogenetic insights provided by compositional transects across the Central American arc: Southeastern Guatemala and Honduras. J. Geophys. Res. 105, 18949–18963.

Woodhead, J.D., Eggins, S., Gamble, J., 1993. High field strength and transition element systematics in island arc and back-arc basin basalts: evidence for multi-phase melt extraction and depleted mantle wedge. Earth Planet. Sci. Lett. 114, 491–504.

Woodhead, J.D., Eggins, S.M., Johnson, R.W., 1998. Magma genesis in the New Britain Island arc: Further insights into melting and mass transfer processes. J. Petrol. 39, 1641–1668.